HEIDAR MORADI

TOPOLOGICAL STATES OF CONDENSED MATTER

SUPERVISOR: BRIAN MØLLER ANDERSEN

B.SC. THESIS

NIELS BOHR INSTITUTE
UNIVERSITY OF COPENHAGEN
2009 - 2010

Abstract

I this project the Thouless-type topological states of matter are investigated, these states are described by a topological invariant which play the role of the order parameter. As an example the TKNN number for the time reversal breaking topological insulators are explicitly constructed and it's significants shown. A few models are taken up and used as examples.

The focus is on the two-dimensional Quantum Spin Hall (QSH) effect and in particular the HgTe/CdTe quantum well. Quantum transport calculations are performed to investigate the role of disorder on these states. This leads to the recently discovered topological Anderson insulator (TAI).

Resume

I dette projekt er topologiske faser af Thouless-typen undersøgt, disse faser er beskrevet af en topologisk invariant der spiller samme rolle som en "ordens parameter". Som eksempel TKNN tallet er tidsomvendings brudte topologiske insulatorer udledt og dets betydning vist. Få simple modeler bliver taget op og brugt som eksempler.

Fokus er på det to-dimentionelle Quantum Spin Hall (QSH) effekt og især HgTe/CdTe kvantebrønde. Kvante transport beregninger er udført for at undersøge påvirkningen af urenheder på disse tilstande. Dette leder til det nygligt opdaget topological Anderson insulator (TAI).

Contents

Preface

1 Introduction

2 Time-reversal breaking band insulators

2.1 Massless Dirac fermions and pseudo-relativistic field theories

As mentioned before a very exiting feature of topological insulators are their low energy excitations. At these energies the dispersion is linear and electron transport is essentially governed by the relativistic Dirac equation for massless fermions. This allows access to subtle and rich physics of quantum electrodynamics in a bench-top experiment [36]. It is of course not true relativistic physics that emerging like a miracle at low energies. For example while the true Dirac equation describes spin of fermions, these pseudo-relativistic equations describe pseudo-spin and the analog to the velocity of light has nothing to do with light. This introduces some differences, for example pseudo-spin do not necessarily couple directly to magnetic fields in contrast to real spin.[1] Later, we will take low energy effective models for granted and work out their properties from there, but I think it is a good idea to see a simple example of such a system in order to get a feeling of how they emerge. Inspired by the amazing experimental work of Novoselov et al. [36], I will present a simple calculation on a single sheet of graphene.

Graphene is made up of carbon atoms, which has six electrons occupying the atomic orbitals $1s^2$, $2s^2$ and $2p^2$. A quick read on Wikipedia reveals that electrons in the $1s^2$ orbital is strongly bonded while the remaining orbitals tends to mix together to form hyberidizated states. This results in σ state covalent bonds, giving rise to a honeycomb lattice (triangular Bravais lattice with a two atom sub lattice), and π orbital with weakly bonded electrons. It is therefore natural to model this in Wannier basis, as localized π orbitals on a honeycomb lattice with nearest neighbor hopping.[2]

A triangular lattice can be described by the primitive lattice vectors $\boldsymbol{a}_1 = \frac{a}{2}\left(1, \sqrt{3}\right)$ and $\boldsymbol{a}_2 = \frac{a}{2}\left(-1, \sqrt{3}\right)$. With a simple drawing it is easy to see that the three nearest neighbors can be described by

$$\boldsymbol{\delta}_1 = \frac{a}{2}\left(1, \frac{1}{\sqrt{3}}\right) \quad \boldsymbol{\delta}_2 = \frac{a}{2}\left(-1, \frac{1}{\sqrt{3}}\right) \quad \boldsymbol{\delta}_3 = \left(0, -\frac{a}{\sqrt{3}}\right), \tag{2.1}$$

where $a = 2.46\,\text{Å}$ for graphene. So the Hamiltonian takes the form

$$H = -t \sum_i \sum_{j=1}^{3} \left(c^\dagger_{\boldsymbol{R}_i + \boldsymbol{\delta}_j} b_{\boldsymbol{R}_i} + b^\dagger_{\boldsymbol{R}_i} c_{\boldsymbol{R}_i + \boldsymbol{\delta}_j} \right), \tag{2.2}$$

[1] Nonetheless I imagine that it is possible to construct a pseudo-relativistic model which couples to magnetic fields like real spin. The point is that the pseudo-spin must behave like a dipole.

[2] This is of course a crude unrealistic model, but it turns out to describe the correct low energy behavior found experimentally.

where for π orbitals we may take $t \approx 2.8$ eV. The b and c operators referee to the two sublattice sites, A and B. Let us assume that our graphene sheet is infinite. Introducing the Fourier transform $c^\dagger_{\boldsymbol{R}_i} = \frac{1}{\sqrt{N}} \sum_{\boldsymbol{k}} e^{-i\boldsymbol{k}\cdot\boldsymbol{R}_i} c^\dagger_{\boldsymbol{k}}$ in (2.2) and using the identity $\frac{1}{N}\sum_i e^{i(\boldsymbol{k}-\boldsymbol{k}')\cdot\boldsymbol{R}_i} = \delta_{\boldsymbol{k}\boldsymbol{k}'}$, we find

$$\begin{aligned} H &= -t \sum_{\boldsymbol{k}} \sum_{j=1}^{3} \left(e^{-i\boldsymbol{k}\cdot\boldsymbol{\delta}_j} c^\dagger_{\boldsymbol{k}} b_{\boldsymbol{k}} + e^{i\boldsymbol{k}\cdot\boldsymbol{\delta}_j} b^\dagger_{\boldsymbol{k}} c_{\boldsymbol{k}} \right) \\ &= \begin{pmatrix} c^\dagger_{\boldsymbol{k}} & b^\dagger_{\boldsymbol{k}} \end{pmatrix} \begin{pmatrix} 0 & -tf(\boldsymbol{k}) \\ -tf^*(\boldsymbol{k}) & 0 \end{pmatrix} \begin{pmatrix} c_{\boldsymbol{k}} \\ b_{\boldsymbol{k}} \end{pmatrix}, \qquad f(\boldsymbol{k}) = \sum_{j=1}^{3} e^{-i\boldsymbol{k}\cdot\boldsymbol{\delta}_j}. \end{aligned} \tag{2.3}$$

In the last equality we have written this in a pseudo-spin form. The sum is easily evaluated $f(\boldsymbol{k}) = e^{i\frac{a}{\sqrt{3}}k_2} + 2e^{-i\frac{a}{2\sqrt{3}}k_2}\cos\left(\frac{a}{2}k_1\right)$ and the eigenvalues are found to be

$$\begin{aligned} \epsilon(\boldsymbol{k}) &= \pm t \left| f(\boldsymbol{k}) \right| = \pm t \sqrt{f(\boldsymbol{k}) f^*(\boldsymbol{k})} \\ &= \pm t \sqrt{1 + 4\cos\left(\frac{a\sqrt{3}}{2}k_2\right)\cos\left(\frac{a}{2}k_1\right) + 4\cos^2\left(\frac{a}{2}k_1\right)}. \end{aligned} \tag{2.4}$$

As seen in figure 2.1a the energy spectrum is not gaped, the valence and the conduction

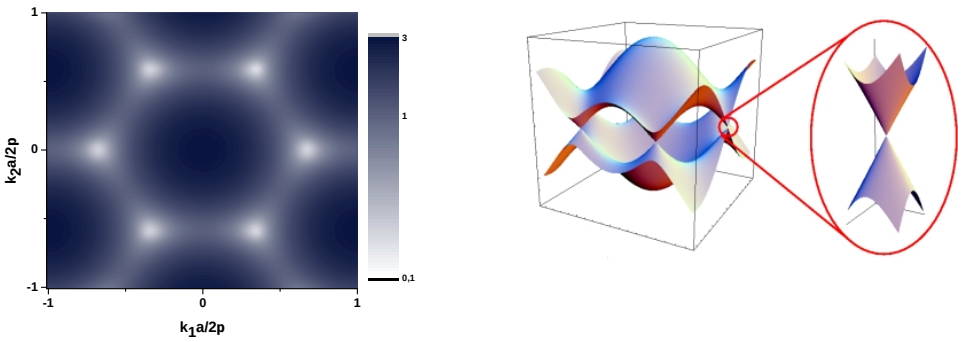

(a) (b)

Figure 2.1: The dispersion relation for an infinite graphene sheet and the Dirac cones giving rise to pseudo-relativistic quasi-particles.

band meets at six points in the Brillouin zone though only two inequivalent, pick for example the points $\boldsymbol{K}_{-1} = (\frac{4\pi}{3a}, 0)$ and $\boldsymbol{K}_{+1} = (-\frac{4\pi}{3a}, 0)$. If the fermi-energi is near $\epsilon \approx 0$ it is sufficient to consider a lowest order expansion around $\boldsymbol{K}_{-1}$ and $\boldsymbol{K}_1$, $f(\boldsymbol{k}) = f(\boldsymbol{K}_\alpha + \boldsymbol{q}) \approx \sum_{j=1}^{3} e^{-i\boldsymbol{K}_\alpha\cdot\boldsymbol{\delta}_j}(1 - i\boldsymbol{q}\cdot\boldsymbol{\delta}_j) = -\sqrt{3}a/2(\alpha q_1 + iq_2)$ for $\alpha = \{-1, 1\}$, leading to

$$\begin{aligned} \epsilon(\boldsymbol{q}) &= \pm t \frac{\sqrt{3}}{2} a \sqrt{q_1^2 + q_2^2} \\ &= \pm \hbar c_* q, \qquad c_* = \frac{ta\sqrt{3}}{2\hbar}. \end{aligned} \tag{2.5}$$

This implies that at low energies, we may consider particles and holes to be massless since the effective mass tensor involves a second derivative (see [30, p. 419]). Recall the dispersion for free relativistic particles $E(k) = \pm\sqrt{c^2\hbar^2k^2 + m^2c^4}$ where for $m = 0 \Rightarrow E(k) = \pm\hbar ck$, which is exactly what we have. In figure 2.1b it is seen how a dirac cone emerges at low energies. Similarly

an effective continuum Hamiltonian can be found from (2.3), written in first quantization

$$h^{\alpha}_{\text{eff}} = t\frac{\sqrt{3}a}{2}\begin{pmatrix} 0 & \alpha q_1 + i q_2 \\ \alpha q_1 - i q_2 & 0 \end{pmatrix}, \tag{2.6}$$

which is very similar to the Dirac equation for massless spin-$\frac{1}{2}$ fermions.[3] The two components describe the two sub-lattices and if spin is taking into account two more components is needed (but the Dirac equation still governs the pseudo-spin, not the real spin).[4]

Putting in numbers, the effective "speed of light" is $c_* \approx 9.1 \cdot 10^5$ m/s and this agrees surprisingly well with the experimental value $c_* \approx 10^6$ m/s. Novoselov et al. [36] further finds Shubnikov-de Haas oscillations and peculiar half-integer QHE where the plateaus are shifted by a half. It could be an interesting exercise to incorporate graphene into the quantum transport machinery build later in this work, to see if this simple tight-binding model describes these effects.

2.2 Integer Quantum Hall Effect and the TKNN number

In time reversal breaking systems a topological invariant can exist, the so-called TKNN number first explored by Thouless et al. [39]. This invariant had great importance in understanding the Quantum Hall (QH) effect, which was among the first discovered topological states of matter. In contrast to the topological numbers describing QSH effect, the TKNN number can be derived in a physical language with little mathematical prerequisites.[5] Therefore I hope after reading this section, the reader will have some idea about where the band topology shows itself. All this topology is not only for the sake of elegance, it has been the source of deep physical understanding and made the path to the theoretical discovery of QSH effect and time reversal invariant topological insulators. This derivation will be a little sketchy and more or less follow the approach of Kohmoto [25].

Consider a 2D non-interacting electron system in a uniform magnetic field perpendicular to the plane, the Schrödinger equation read

$$H\psi(\boldsymbol{r}) = \left[\frac{1}{2m}(\boldsymbol{p} + e\boldsymbol{A})^2 + U(\boldsymbol{r})\right]\psi(\boldsymbol{r}) = E\psi(\boldsymbol{r}), \tag{2.7}$$

where $\boldsymbol{p} = -i\hbar\boldsymbol{\nabla}$ and $\boldsymbol{A}$ ensures local $U(1)$ gauge symmetry. Let $\boldsymbol{R} = n\boldsymbol{a} + m\boldsymbol{b}$, for $(n,m) \in \mathbb{Z}^2$, be the Bravais lattice vector and assume that $U(\boldsymbol{r})$ is periodic in this lattice, $U(\boldsymbol{r}+\boldsymbol{R}) = U(\boldsymbol{r})$. Furthermore, for simplicity assume that $\boldsymbol{a}$ and $\boldsymbol{b}$ are perpendicular and point along the x and y axes, respectively. Define the discrete translation operator

$$T_{\boldsymbol{R}} f(\boldsymbol{r}) = \exp\left\{(i/\hbar)\boldsymbol{R}\cdot\boldsymbol{p}\right\} f(\boldsymbol{r}) = f(\boldsymbol{r}+\boldsymbol{R}). \tag{2.8}$$

The magnetic field is perpendicular to the plane and the system is clearly translational invariant, but a quick look at equation (2.7) reveals that the Hamiltonian is not invariant under $T_{\boldsymbol{R}}$.

[3] This can be written in the form $h^{\alpha}_{\text{eff}} = \hbar c_* \boldsymbol{d}\cdot\boldsymbol{\sigma}$, with $\boldsymbol{d} = (q_1, -q_2, 0)$ and $\boldsymbol{\sigma}$ are the Pauli matrices.

[4] In practice one probably needs to use a Hamiltonian like $h^{-1}_{\text{eff}} \oplus h^{+1}_{\text{eff}}$.

[5] In my opinion the derivation becomes most transparent, intuitive and almost trivial when formulated using fiber bundle theory. But of course it requires lots of time and hard work to build up the intuition and therefore I have avoided it here. But I encourage all physicist to learn these beautiful mathematical theories (differential geometry, algebraic topology and Lie group theory), please spread the word.

The problem occurs because the vector potential $\boldsymbol{A}(\boldsymbol{r})$ is not uniform even though the magnetic field is (because $\boldsymbol{B} = \boldsymbol{\nabla} \times \boldsymbol{A}$) and $\boldsymbol{A}(\boldsymbol{r})$ may not in general be periodic. But since a translation cannot alter the physics, it must only differ by a gradient of a scalar function $\boldsymbol{A}(\boldsymbol{r}) = \boldsymbol{A}(\boldsymbol{r}+\boldsymbol{R}) + \boldsymbol{\nabla} g(\boldsymbol{r})$. This problem can be solved by choosing the symmetric gauge[6] $(\boldsymbol{B} \times \boldsymbol{r})/2$ and defining the magnetic translation operator

$$\begin{aligned} \hat{T}_{\boldsymbol{R}} &= \exp\left\{(i/\hbar)\boldsymbol{R} \cdot [\boldsymbol{p} + e(\boldsymbol{r} \times \boldsymbol{B})/2]\right\} \\ &= T_{\boldsymbol{R}} \exp\left\{(ie/\hbar)(\boldsymbol{B} \times \boldsymbol{R}) \cdot \boldsymbol{r}/2\right\}, \end{aligned} \tag{2.9}$$

which is just (2.8) with the gauge field added to the momentum. One can now show that $\left[\hat{T}_{\boldsymbol{R}}, H\right] = 0$. There is still one problem the translation operators do not commute with each other, a calculation shows that[7] $\hat{T}_{\boldsymbol{a}} \hat{T}_{\boldsymbol{b}} = \exp(2\pi i \phi) \hat{T}_{\boldsymbol{b}} \hat{T}_{\boldsymbol{a}}$ where $\phi = (eB/\hbar)ab$ is the number of magnetic flux in the unit cell. When ϕ is a rational number p/q we can take out an Abelian subgroup. We can enlarge the unit cell (magnetic unit cell) by defining a new Bravais lattice vector[8]

$$\boldsymbol{R}' = n(q\boldsymbol{a}) + m\boldsymbol{b}$$

and therefore there will be p (integer) magnetic flux quanta in each unit cell. It is now possible diagonalize H and $\hat{T}_{\boldsymbol{R}'}$ simultaneously. Since Abelian groups have only one dimensional representations one can show that $\hat{T}_{q\boldsymbol{a}}\psi = e^{ik_1 qa}\psi$ and $\hat{T}_{\boldsymbol{b}}\psi = e^{ik_2 b}\psi$, where the generalized crystal momenta are restricted in the magnetic Brillouin zone: $0 \le k_1 \le 2\pi/qa$ and $0 \le k_2 \le 2\pi/b$. We can now label eigenfunctions of H with the good quantum numbers k_1 and k_2 plus an additional band index α, thus in Bloch form we have $\psi^{(\alpha)}_{\boldsymbol{k}}(\boldsymbol{r}) = e^{i\boldsymbol{k}\cdot\boldsymbol{r}} u^{(\alpha)}_{\boldsymbol{k}}(\boldsymbol{r})$.[9] From equation (2.7) one can find an effective $\boldsymbol{k}$ dependent Hamiltonian for $u^{(\alpha)}_{\boldsymbol{k}}$

$$\hat{H}(\boldsymbol{k}) u^{(\alpha)}_{\boldsymbol{k}} = \frac{1}{2m}\left(-i\hbar\boldsymbol{\nabla} + \hbar\boldsymbol{k} + e\boldsymbol{A}\right)^2 u^{(\alpha)}_{\boldsymbol{k}} + U(\boldsymbol{r}) u^{(\alpha)}_{\boldsymbol{k}} = E^{\alpha} u^{(\alpha)}_{\boldsymbol{k}},$$

where the $\boldsymbol{k}$ dependence of the energy is implied. To make a connection to Quantum Hall Effect, imagine we apply a weak electric field such that we are in the linear response regime. The Hall conductivity perpendicular to the applied electric field may be calculated as[10]

$$\sigma_{xy} = -ie^2\hbar \sum_{E^{\alpha} < E_F} \sum_{E_F < E^{\beta}} \frac{(v_y)_{\alpha\beta}(v_x)_{\beta\alpha} - (v_x)_{\alpha\beta}(v_y)_{\beta\alpha}}{\left(E^{\alpha} - E^{\beta}\right)^2}, \tag{2.10}$$

where $(v_i)_{\alpha\beta} = \frac{1}{\hbar}\left\langle \alpha \left| \frac{\partial \hat{H}}{\partial k_i} \right| \beta \right\rangle$, $i = 1, 2$, are the usual semi-classical velocities as derived from $\boldsymbol{k}\cdot\boldsymbol{p}$ theory (see for example [30, P. 417]). After some calculations one finds that the conductivity per fully occupied band is given as[11]

$$\sigma^{(\alpha)}_{xy} = \frac{e^2}{h} \frac{1}{2\pi} \int \mathrm{d}^2\boldsymbol{k} \left[\boldsymbol{\nabla}_{\boldsymbol{k}} \times \hat{\boldsymbol{A}}^{(\alpha)}(\boldsymbol{k})\right]_3, \tag{2.11}$$

[6] Other choices of the gauge will also work, for example the Landau gauge is used in the original TKNN paper [39].

[7] In fact I do not get the 2π when calculating this. If it is me making a mistake, or Kohmoto [25] is not important since with a small modification everything else follows.

[8] Again, other choices would also work. They would lead to different results, but physically equivalent.

[9] But with some generalized Bloch conditions $u_{k_1,k_2}(\alpha)(x+qa, y) = e^{-i\pi py/b} u^{(\alpha)}_{k_1,k_2}(x, y)$ and $u_{k_1,k_2}(\alpha)(x, y+b) = e^{i\pi px/qa} u^{(\alpha)}_{k_1,k_2}(x, y)$.

[10] This formula is called the Nakao-Kubo formula and is different from the from Kubo formula based on current-current correlations evaluated in thermal equilibrium (see [7, Chapter 6]).

[11] More explicitly the expression is given by $\sigma^{(\alpha)}_{xy} = \frac{e^2}{h}\frac{1}{2\pi i}\int \mathrm{d}^2\boldsymbol{k} \int \mathrm{d}^2\boldsymbol{r} \left(\frac{\partial u^{(\alpha)*}_{\boldsymbol{k}}}{\partial k_2} \frac{\partial u^{(\alpha)}_{\boldsymbol{k}}}{\partial k_1} - \frac{\partial u^{(\alpha)*}_{\boldsymbol{k}}}{\partial k_1} \frac{\partial u^{(\alpha)}_{\boldsymbol{k}}}{\partial k_2} \right)$. To avoid confusion, note that our definition of $\hat{\boldsymbol{A}}^{(\alpha)}(\boldsymbol{k})$ i different from [25].

where $[\quad]_3$ stands for the third component, the integral is over the magnetic Brillouin zone and the vector field $\hat{\boldsymbol{A}}^{(\alpha)}(\boldsymbol{k})$ is defined as

$$\hat{\boldsymbol{A}}^{(\alpha)}(\boldsymbol{k}) = -i\int \mathrm{d}^2\boldsymbol{r}\, u_{\boldsymbol{k}}^{(\alpha)*}\boldsymbol{\nabla}_{\boldsymbol{k}} u_{\boldsymbol{k}}^{(\alpha)} = -i\left\langle u_{\boldsymbol{k}}^{(\alpha)}\right|\boldsymbol{\nabla}_{\boldsymbol{k}}\left|u_{\boldsymbol{k}}^{(\alpha)}\right\rangle. \tag{2.12}$$

Equation (2.11) is the famous TKNN result. As the reader may have suspected from equation (2.12), there is a connection to the Berry phase.[12] There is now a crucial point to observe, the magnetic Brillouin zone is homeomorphic (topologically equivalent) to a torus T^2.[13] This is due to the periodicity, the points at $k_1 = 0$ ($k_2 = 0$) is to be identified with $k_1 = 2\pi/qa$ ($k_2 = 2\pi/b$). Just fold the square to connect identical sides. If Stokes' theorem is used to change equation (2.11) into a line integral one finds that $\sigma_{xy} = 0$ since a torus does not have any boundaries. This disappointing result is of course in contrast to experimental observations. Here is where topology comes into the picture.

First notice that a phase transformation

$$u_{\boldsymbol{k}}^{(\alpha)\prime}(\boldsymbol{r}) = u_{\boldsymbol{k}}^{(\alpha)}(\boldsymbol{r})e^{if(\boldsymbol{k})} \Rightarrow \hat{\boldsymbol{A}}^{(\alpha)\prime}(\boldsymbol{k}) = \hat{\boldsymbol{A}}^{(\alpha)}(\boldsymbol{k}) + \boldsymbol{\nabla}_{\boldsymbol{k}} f(\boldsymbol{k}), \tag{2.13}$$

as is seen from equation (2.12). This is a local gauge transformation in the magnetic Brillouin zone but global in physical space, and it implies that $\hat{\boldsymbol{A}}^{(\alpha)}(\boldsymbol{k})$ can be thought of as a $U(1)$ gauge field with a corresponding "magnetic field" $\hat{\boldsymbol{B}}^{(\alpha)}(\boldsymbol{k}) = \boldsymbol{\nabla}_{\boldsymbol{k}} \times \hat{\boldsymbol{A}}^{(\alpha)}(\boldsymbol{k})$.[14] More importantly the conductivity (2.11) is invariant under such transformations. Stokes' theorem can only be used as we did, if $\hat{\boldsymbol{A}}^{(\alpha)}(\boldsymbol{k})$ can be defined globally on T^2.[15] But since the base space T^2 is non-contractible and non-simply connected[16] it is possible to have a non-trivial bundle (where continuous Bloch functions cannot be defined globally). But T^2 can be split into several contractible open sets with different phases assigned to each and then "glued" together through a $U(1)$-transition function. Then one can use Stokes' theorem in equation (2.11) locally and the phase mismatch at the boundaries of the different open sets contributes with a non-zero Hall conductivity. More importantly when formulated on fiber bundles, the quantity $c_1 = \frac{-1}{2\pi}\int \mathrm{d}^2\boldsymbol{k}\left[\boldsymbol{\nabla}_{\boldsymbol{k}} \times \hat{\boldsymbol{A}}^{(\alpha)}(\boldsymbol{k})\right]_3$ is identified as the first Chern number which is a well known (among differential/algebraic topologists) topological invariant. This explains the Hall quantization.

A more elementary and explicit discussion of the last part is given in [25], but I have chosen not to include it due to lack of space and because i do not find the argument transparent enough for the reader to benefit from.

Finally the Hall conductivity as measured experimentally is $\sigma_{xy} = \nu e^2/h$, with the filling factor given as

$$\nu = \sum_{\alpha:\text{filled}} \int \frac{\mathrm{d}^2\boldsymbol{k}}{2\pi} B_z^{(\alpha)}(\boldsymbol{k}). \tag{2.14}$$

[12] The discussion of the Berry phase has been neglected, but for interested readers I recommend Berry's original paper [5] or the book [42]. Readers interested in a geometric fiber bundle formulation see [6] or [34] for different approaches.

[13] A torus is a surface of a doughnut, inner tube, or bagel, depending on the readers background.

[14] This field can be explicitly constructed as a connection on a $U(1)$ principal bundle with T^2 as the base space, exactly like the electromagnetic gauge field (with the spacetime as the basespace).

[15] A general theorem states that a principal bundle is trivial iff it has a global section. See for example [3, 34, 12]. Trivial means that it is of the form $T^2 \times U(1)$ globally and therefore not "twisted".

[16] It is intuitively seen that the first homotopy group $\pi_1(T^2)$ is isomorphic to $\mathbb{Z} \times \mathbb{Z}$ and T^2 is therefore not contractible nor simply connected.

This result shows that only by a change of the band topology, a phase transition in a QH system can occur and the number ν plays the role of an order parameter.[17]

2.3 Topological Invariants and edge states

Not long after the discovery of Quantum Hall Effect Laughlin [26] presented a very elegant and general explanation (now refereed to as *Laughlin's gauge argument*) of why the Hall conductance is quantized in exact integer multiples of e^2/h. Halperin [17] extended this argument and emphasized on a very important implication about the existence of extended quasi-one dimensional states at the edge which carry current and do not become localized in the presence of a disorder potential of moderate strength. This further implies that the Chern number represents the number of chiral gapless edge states going around the sample edge. Namely the existence of the gapless edge states is guaranteed by the Chern number. This comes from the Laughlin argument; roll the two-dimensional system into an open cylinder by attaching two edges on the opposite sides, and let a flux Φ penetrate the hole. The flux Φ is to be increased adiabatically from 0 to a flux quantum. Then the number of electrons carried from one edge of the cylinder to the other is equal to the Chern number. These carried electrons are on the gapless edge states. Thus we can establish the correspondence between the number of chiral edge states and the Chern number.[18] For the details of these arguments, the reader is referred to the original papers.

While we are at it let us introduces yet another twist in the story which was very important in the discovery of the Quantum Spin Hall effect. In 1988 Haldane [16] introduced a simple model based on the honeycomb lattice which showed that in principle one can have Quantum Hall effect without any magnetic field, thus no Landau levels. The main idea is to have another (intrinsic or extrinsic) mechanism to break the time reversal symmetry, because the Chern number is odd under a time reversal transformation and it can therefore be non-zero only if this symmetry is broken. The Hamiltonian reads as follows

$$H_{\text{Haldane}} = t_1 \sum_{\langle i,j\rangle} c_i^\dagger c_j + t_2 \sum_{\langle\langle i,j\rangle\rangle} e^{-i\nu_{ij}\phi} c_i^\dagger c_j + M \sum_i \xi_i c_i^\dagger c_i. \tag{2.15}$$

The first term is a nearest neighbor tight-binding term giving rise to the massless dirac fermions discussed earlier. The second term introduces a complex next-nearest neighbor hopping to break the time reversal symmetry.[19] Here $\nu_{ij} = \text{sgn}(\hat{\boldsymbol{d}}_1 \times \hat{\boldsymbol{d}}_2) = \pm 1$, where $\hat{\boldsymbol{d}}_1$ and $\hat{\boldsymbol{d}}_2$ are unit vectors along the two bonds, which constitute the next-nearest neighbor hopping. Finally the last term is a staggered on-site potential where ξ_i is ± 1 depending on the i-th site being the A or B sublattice, the effect of this term is to create a bulk gab. Haldane [16] was then interested to understand phase transitions in this model and to see if there exists any Quantum Hall phases. This means that we have to calculate the first Chern number, but this is not an easy task using Bloch functions.[20] Instead one can observe that when $\phi = 0$, the Hamiltonian

[17] The Chern number can also be formulated for many-body interacting systems like the fractional quantum Hall effect, using twisted-boundary conditions [35]. But this discussion is beyond the scope of this project and rather irrelevant.

[18] Edge transport in the Quantum Hall effect has been well studied. X. G. Wen discovered that the edge states in the Fractional Quantum Hall effect is, at low energies, governed by a chiral Luttinger liquid. This has been a source of rich and interesting physics.

[19] Recall the time-reversal operator which, including spin, may be written as $\theta = -i\sigma_y K$. K stands for complex conjugation.

[20] One can show that the TKNN formula still works without a magnetic field, but usually (in standard band insulators) ν is zero due to the trivial topology of the occupied bands.

is time reversal invariant and the Chern number is therefore $\nu = 0$. The trick is now to see how ν changes when a parameter is changed, it turns out that the boundary of the different phases is described by M vs. $\pm 3\sqrt{3}t_2 \sin\phi$. For a simple and elegant argument see Murakami [32].[21] The phase diagram is shown in figure 2.2 and it is seen that there are three different

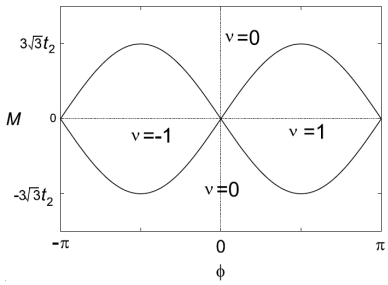

Figure 2.2: Phase diagram of Haldane's model, ν represents the Chern number.

phases, one topologically trivial and two topologically non-trivial. It is interesting to compare the band structure of these different phases and to see how the gapless edge states, which must exist according to Laughlin's gauge argument, reveal themselves. For this we need a geometry with edges. We have chosen a zig-zag geometry which is infinite along one axes and therefore have two edges, let us call them left and right (other choices, like arm-chair edges, gives qualitatively the same results). One has to write the Hamiltonian in equation (2.15) in terms of the zig-zag geometry and fourier transform along the infinite direction, then derive an eigenvalue equation to be solved. More details are given in the next section where something similar is done. Spin has been neglected since it only contributes with a unimportant degeneracy. In figure 2.3 the energy spectrum for three different values of ϕ is shown, with

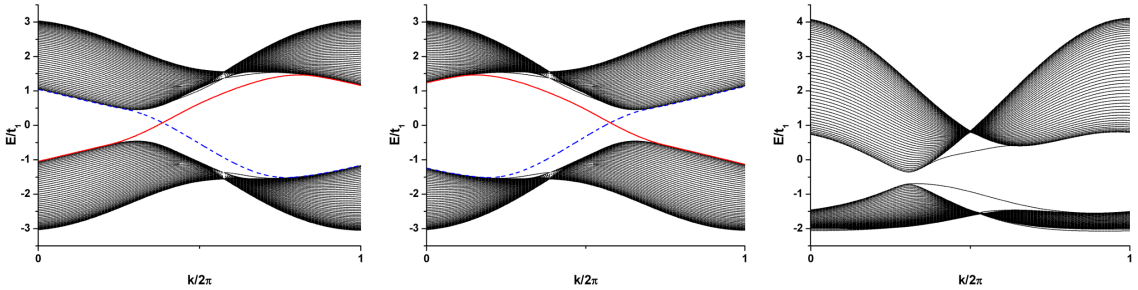

(a) $\phi = \pi/2$ **(b)** $\phi = -\pi/2$ **(c)** $\phi = \pi/8$

Figure 2.3: The energy spectrum of Haldane's model in zig-zag geometry with the values $M/t_1 = 0.55$ and $t_2/t_1 = 1/(3\sqrt{3})$. The shaded areas are the energy bands of the bulk and the colored lines are the spectrum of the edge states. The red (solid) and blue (dashed) lines mean that the edge states are localized near the left and right edges, respectively.

fixed $M/t_1 = 0.55$ and $t_2/t_1 = 1/(3\sqrt{3})$ (compare with figure 2.2). The red (solid) and blue (dashed) lines mean that the corresponding eigenvectors of equation (2.15) are localized near the left and right edges, respectively. There have been experimenting with many different set

[21] The idea is that while the topological number involves an integral over the whole Brillouin zone, changes happens locally. When $\nu = 0$ there is a energy gap and the idea is to observe when the gap closes and a Dirac fermion is formed.

of parameters and a qualitative change happens only with phase transitions which follow very accurately the diagram in figure 2.2.[22]

In figure 2.3c the Chern number is $\nu = 0$ and a energy gap is seen, which is characteristic for (topologically trivial) band insulators. Something interesting happens in figure 2.3a where now $\nu = 1$. While the bulk of the system is gaped, there are a gapless state near each edge which are counter propagating (recall that the slope is proportional to the velocity of the Dirac fermions, in the semi-classical picture). This is as predicted by Lauligh's gauge argument. It is worth noticing that for increasing k the red (blue) band is starting in the lower (upper) bulk band and ending in the upper (lower) bulk band. This "inverted-ness" implies that there are some sort of non-trivial band topology, which the number $\nu = 1$ indeed verifies. In figure 2.3b we now have $\nu = -1$ and we again observe one current-carrying state at each edge. But the velocity of the edge states have now changed sign, which again implies a change of topology. It is not possible to continuously deform one of these spectrums into another, thus they are part of different topological classes.

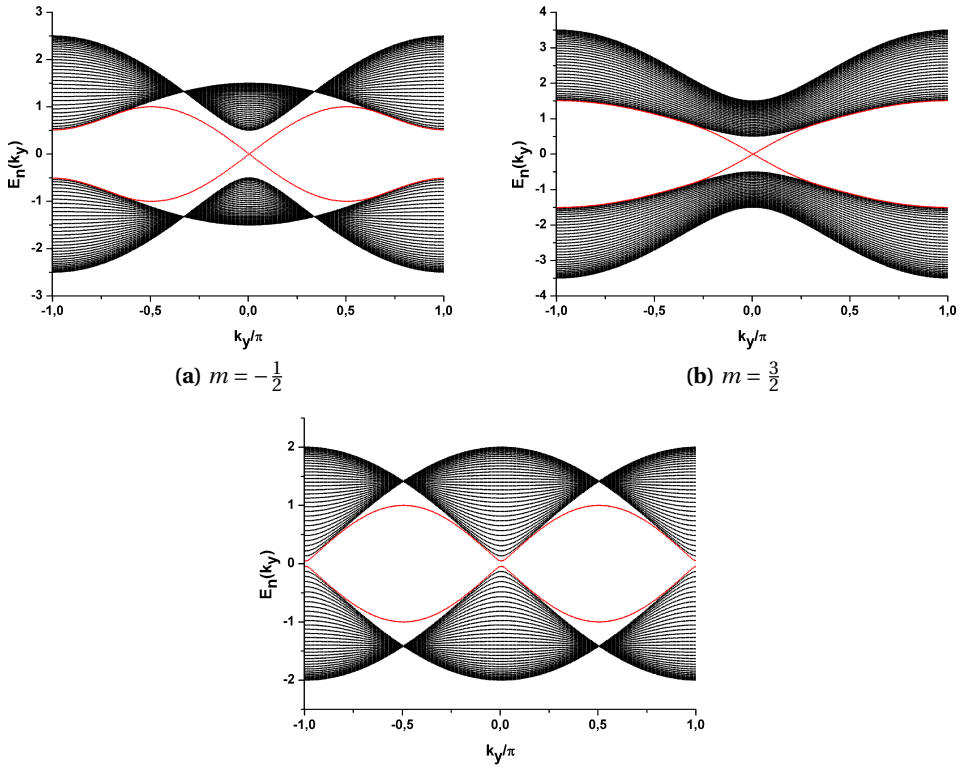

(a) $m = -\frac{1}{2}$ **(b)** $m = \frac{3}{2}$

(c) $m = 0$

Figure 2.4

A longer and deeper discussion of these topological time-reversal breaking insulators and their connection to topological quantum field (Chern-Simon's) theory, the Berry phase and Laughlin's gauge argument has been neglected. But a few figures I intended to use for this purpose can be seen in figure 2.4, now I have spend time making them. I recommend the reader to take a short artistic break in order enjoy this aesthetic piece of post-modern art.

[22] I have not been able to find anything in the literature to compare figure 2.3 with directly. But when $t_2 = M = 0$ we actually have a zig-zag graphene nano-ribbon. The dispersion is in good agreement with the graphene literature (see [41]). Due to this and other reasons, I believe figure 2.3 is correct.

3 Quantum Spin Hall Effect

3.1 The Z_2 topological number and Kane-Mele model

The QSH effect is a phenomena similar to the QH effect but with some key differences. The QSH insulator state is invariant under time reversal, has a excitation gap in the two-dimensional bulk, but with topologically protected gapless edge states that lie inside the bulk insulating gap. The edge states have a distinct helical property: two states with opposite spin-polarization counter propagate at a given edge, thus the name helical edge states. The edge states come in pairs and due to Kramers degeneracy theorem the crossing of their energy levels at special points in the Brillouin zone is secured, these points must remain degenerate because of the time-reversal symmetry. Since the Chern number is odd under time-reversal transformations it must vanish in QSH systems, but it turns out that another topological order exists.

The simplest way of realizing the QSH state is by superposing two QH systems with opposite spin, or put in another way, a QH system with its time-reversed counterpart. Use for example the Haldane model to construct the Hamiltonian

$$H = \begin{pmatrix} H_\uparrow & 0 \\ 0 & H_\downarrow \end{pmatrix} = \begin{pmatrix} H_{\text{Haldane}}(\phi = -\pi/2) & 0 \\ 0 & H^*_{\text{Haldane}}(\phi = \pi/2) \end{pmatrix}.$$

The superposition (more precisely, direct sum) of the down-spin QH subsystem ($\sigma_{xy} = e^2/h$) and the up-spin QH subsystem ($\sigma_{xy} = -e^2/h$) results in $\nu = \nu_\uparrow + \nu_\downarrow = 0$ (see figure 2.2). While the sum vanishes due to time-reversal symmetry, the difference $\nu_\uparrow - \nu_\downarrow \equiv 2\nu_s$ is non-zero and can be used to define a "spin Chern number", ν_s, that counts number of time-reversed (Kramer's) pairs of edge modes. In this simple example s_z is conserved, which may not be the case in a real system where spin-coupling terms will mix the two sub-systems. The question is what happens when s_z is no longer a good quantum number. To answer this question Kane and Mele [23, 22] proposed a model on the honeycomb lattice, inspired by (2.15)

$$H = -t \sum_{\langle ij \rangle} c_i^\dagger c_j + i\lambda_{SO} \sum_{\langle\langle ij \rangle\rangle} \nu_{ij} c_i^\dagger s_z c_j + i\lambda_R \sum_{\langle ij \rangle} c_i^\dagger \left(\boldsymbol{s} \times \hat{\boldsymbol{d}}_{ij}\right)_z c_j + \lambda_v \sum_i \xi_i c_i^\dagger c_i. \tag{3.1}$$

The second terms is a mirror symmetric spin-orbit terms while the third term is a so-called Rashba term which explicitly violates the $z \to -z$ mirror symmetry, and will arise due to a perpendicular electric field or interaction with a substrate. The key ingredient turns out to be the time-reversal symmetry, which gives rise to the Kramer's pairs at $\boldsymbol{k}$ and $-\boldsymbol{k}$. Kane and Mele [23] found out that a Z_2 topological number can be formulated, corresponding to if there are an odd or even number of time-reversed pairs on each edge.[1] If odd number of pairs, the system is in the QSH phase otherwise the system is an trivial insulator. So even if spin is not conversed the QSH phase is still well defined, since an odd number of time reversed pairs are

[1] Again most of the discussion has been neglected, interested readers might start with [23, 38, 13].

on each edge. The edge states are therefore more fundamental than the spin Hall effect and a more appropriate name would be *topological Z_2 insulator*. The Z_2 topological number, in it's different forms, has been used as a theoretical tool to track down realistic systems exhibiting the QSH state. This has proven to be a very successful tool and already various candidates has been found and experimentally realized.

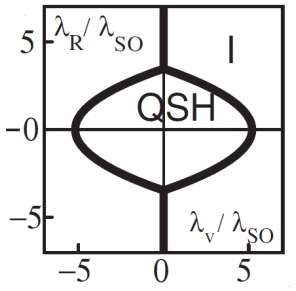

(a) The phase diagram for the Kane-Mele model, see [23] for details.

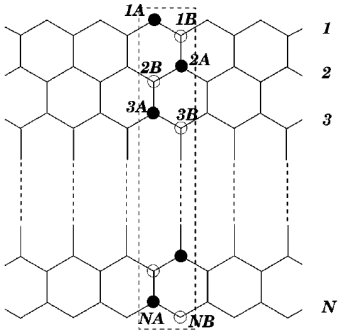

(b) Structure of finite honeycomb lattice with zig-zag edges. The rectangle with the dashed line is the unit cell.

Figure 3.1

To see any edge states in the Kane-Mele model, we need a geometry with edges. Just like the last section we will choose a finite lattice in one direction with zig-zag edges while infinite in the other. In figure 3.1b the structure of the lattice is shown and a unit cell is marked by dashed lines. Now define the an operator $c^\dagger_\alpha(i)$ ($c_\alpha(i)$), which creates (annihilates) a fermion on the site i and unit cell α.[2] Now it is straightforward to write equation (3.1) in this geometry, for example

$$-t\sum_{\langle ij\rangle} c_i^\dagger c_j = -t\sum_{\alpha,m}\Big[c_\alpha^\dagger(mA)\big\{c_\alpha(mB)+c_{\alpha-1}(mB)+c_\alpha(m-1B)\big\}+h.c.\Big]$$

and

$$\begin{aligned} i\lambda_{SO}\sum_{\langle\langle ij\rangle\rangle}\nu_{ij}c_i^\dagger s_z c_j = i\lambda_{SO}\sum_{\alpha,m} c_\alpha^\dagger(mA)s_z\big\{&c_\alpha(m-1A)+c_{\alpha-1}(m+1A)+c_{\alpha+1}(mA)\\ &-c_{\alpha-1}(mA)-c_{\alpha+1}(m-1A)-c_\alpha(m+1A)\big\}\\ &+\text{same for sublattice B,}\end{aligned}$$

and similarly for the other terms. Because of translational invariance we introduce the Fourier transform $c^\dagger_\alpha(i)=\frac{1}{\sqrt{L}}\sum_k e^{ikr_\alpha}c^\dagger_k(i)$. Inspired by the method used in [41], we take a general one-particle state

$$|\Psi(k)\rangle=\sum_m\left[\psi_{mA}(k)c^\dagger_{mA}(k)+\psi_{mB}(k)c^\dagger_{mB}(k)\right]|0\rangle,$$

where $|0\rangle$ represents the ground state, and require that it must satisfy $H(k)|\Psi(k)\rangle=\epsilon(k)|\Psi(k)\rangle$. These straightforward, though tedious, calculations leads to a set of coupled algebraic equa-

[2] Spin is included, $c^\dagger_\alpha(i)=\left(c^\dagger_{\alpha\uparrow}(i),c^\dagger_{\alpha\downarrow}(i)\right)$.

tions[3]

$$\epsilon\psi_{mA\sigma} = p_1\psi_{mB\sigma} + t\psi_{m-1B\sigma} + \text{sign}(\sigma)p_3\left[\psi_{m+1A\sigma} + \psi_{m-1A\sigma}\right] + \left[\lambda_v - \text{sign}(\sigma)p_2\right]\psi_{mA\sigma}, \quad (3.2)$$

$$\epsilon\psi_{mB\sigma} = p_1\psi_{mA\sigma} + t\psi_{m+1A\sigma} - \text{sign}(\sigma)p_3\left[\psi_{m+1B\sigma} + \psi_{m-1B\sigma}\right] + \left[\text{sign}(\sigma)p_2 - \lambda_v\right]\psi_{mB\sigma}, \quad (3.3)$$

where $\sigma \in \{\uparrow, \downarrow\}$, $\text{sign}(\uparrow) = 1$, $\text{sign}(\downarrow) = -1$, $p_1 = 2t\cos\left(\frac{\sqrt{3}}{2}ka\right)$, $p_2 = 2\lambda_{SO}\sin\left(\sqrt{3}ka\right)$ and finally $p_3 = 2\lambda_{SO}\sin\left(\frac{\sqrt{3}}{2}ka\right)$. In figure 3.2 these equations have been solved and some representatives are shown.

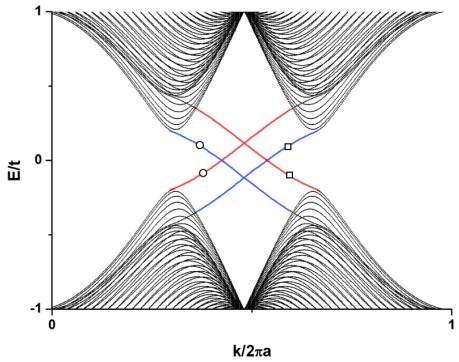

(a) Energy dispersion for the Kane-Mele model in the QSH phase for $\lambda_R = 0$, $\lambda_{SO} = 0.06$, $\lambda_v = 0.12$, $t = 1$. Red and blue color are for spin up and down, respectively and the circle/box are for different edges.

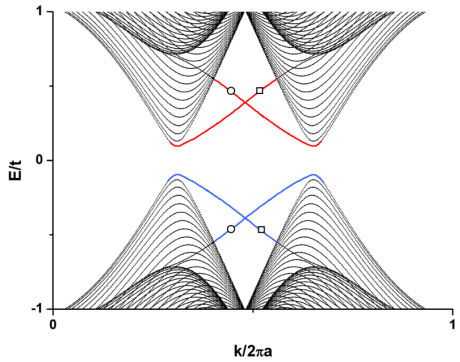

(b) Energy dispersion for the Kane-Mele model in the topologically trivial insulator phase for $\lambda_R = 0$, $\lambda_{SO} = 0.06$, $\lambda_v = 0.4$, $t = 1$.

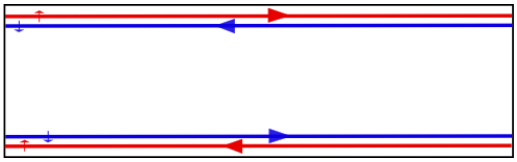

(c) Edge states for the spectrum in figure (a). If $\lambda_R \neq 0$ spin would not be conserved, but one time-reversed pair on each edge would still exist.

Figure 3.2

3.2 HgTe/CdTe Quantum Wells

A very interesting and realistic QSH system was proposed by Bernevig et al. [4]. They considered a HgTe/CdTe quantum well and using a realistic 8 band Kane model (based on $\boldsymbol{k}\cdot\boldsymbol{p}$-theory) they observed that at a critical well thickness d_c the electron and hole bands are inverted (see figure 3.3). For $d < d_c$ the system is topologically trivial but for $d > d_c$ the system is in the QSH phase. A effective 4-band model can be derived which contains all the relevant

[3] For simplicity we show the case $\lambda_R = 0$.

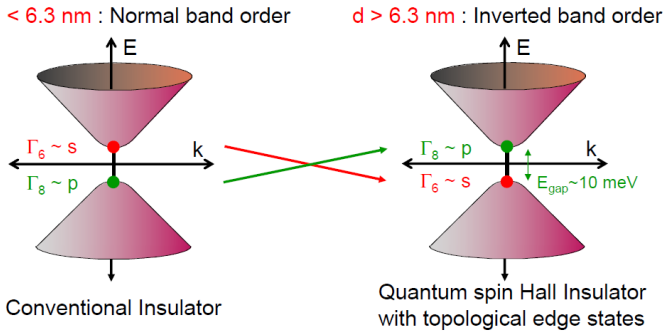

Figure 3.3

topological information (see [4] using the Kane model, or [24] using symmetry arguments)

$$H = \begin{pmatrix} h(\boldsymbol{k}) & 0 \\ 0 & h^*(-\boldsymbol{k}) \end{pmatrix} \tag{3.4}$$

$$h(\boldsymbol{k}) = \epsilon(\boldsymbol{k}) I_{2\times 2} + \boldsymbol{d}(\boldsymbol{k}) \cdot \boldsymbol{\sigma} \tag{3.5}$$

$$\epsilon(\boldsymbol{k}) = C - D(k_x^2 + k_y^2) \tag{3.6}$$

$$\boldsymbol{d}(\boldsymbol{k}) = \big(Ak_x, -Ak_y, M(\boldsymbol{k})\big) \tag{3.7}$$

$$M(\boldsymbol{k}) = M - B(k_x^2 + k_y^2) \tag{3.8}$$

The parameters A, B, C, D and M depends on the QW geometry and can either be derived from the Kane model or found experimentally. The Hamiltonian can be seen as describing two massive Dirac fermions with a $\boldsymbol{k}$ dependent mass $M(\boldsymbol{k})$.[4] Most of the following sections are devoted to explore some of the physical properties of this model.

We are mostly interested in studying this model numerically and for this purpose it is most convenient to use a simplified tight-binding representation on a square lattice which will give us the dispersions over the entire Brillouin zone torus. This enables us to reduce the problem to simple linear algebra, rather than differential equations in the continuum model.[5] A lattice regularization can be obtained by the substitutions $k_i \to a^{-1}\sin(k_i a)$ and $k_i^2 \to 2a^{-2}(1-\cos(k_i a))$, where $i \in \{x, y\}$, so we now have

$$\epsilon(\boldsymbol{k}) = C - 2Da^{-2}[2 - \cos(k_x a) - \cos(k_y a)], \tag{3.9}$$

$$\boldsymbol{d}(\boldsymbol{k}) = \big(Aa^{-1}\sin(k_x a), -Aa^{-1}\sin(k_y a), M(\boldsymbol{k})\big), \tag{3.10}$$

$$M(\boldsymbol{k}) = M - 2Ba^{-2}[2 - \cos(k_x a) - \cos(k_y a)], \tag{3.11}$$

which reduces to the continuum model for small $\boldsymbol{k}$. Now our model consists of a square lattice with four orbitals $|s,\uparrow\rangle$, $|p_x + ip_y,\uparrow\rangle$, $|s,\downarrow\rangle$, $|-(p_x - ip_y),\downarrow\rangle$ on each site [4]. The upper 2×2 sub-block is for spin up, while the lower 2×2 sub-block is for the time-reversed spin-down partner.[6] As discussed by König et al. [24], this lattice Hamiltonian has several critical points

[4] It is straightforward to find the dispersion $E_\pm = \epsilon(\boldsymbol{k}) \pm \sqrt{d_\alpha d^\alpha} = \epsilon(\boldsymbol{k}) \pm \sqrt{A^2k^2 + M(\boldsymbol{k})^2}$. Besides an unimportant energy shift $\epsilon(\boldsymbol{k})$, this is the dispersion of a massive relativistic particle.

[5] This is a very common trick in this sort of problems, see for example Datta [9]. It is also related to the finite difference method, which is a widely used technique in solving differential equations numerically.

[6] Spin is conserved in this model. In reality spin mixing terms exists but they have little influence on the physics [4, 24].

but only one in the low-energy regime (for which it is valid). As we discussed in the last section this model can be thought of as a superposition of two Quantum Hall systems. It turns out that the Hall conductance of the massive Dirac model, $\sigma_{xy} = c_1 e^2/h$ with $c_1 \in \mathbb{Z}$, is given by the Pontryagin widing number[7]

$$c_1 = -\frac{1}{8\pi^2}\int \frac{d^2k}{(2\pi)^2}\epsilon_{abc}\epsilon_{ij}\frac{d_a\partial_i d_b\partial_j d_c}{d^3},$$

where ϵ_{abc} and ϵ_{ij} are the totally asymmetric Levi-Civita symbols.[8] Numerical integration show that $c_1 = 0$ for $M/2B < 0$ and $c_1 = \pm 1$ for $0 < M/2B < 2$, where + (−) corresponds to the $h(\boldsymbol{k})$ ($h^*(-\boldsymbol{k})$) sub-block. In physical systems B is negative and large compared to M, thus the condition $M < 0$ implies that the system is in the QSH phase and for $M > 0$ in the topologically trivial phase. In the literature the parameter M is sometimes referred to as the topological mass.

Without loss of generality take $a = 1$, which is nothing but a redefinition of units. It is convenient to rewrite the Hamiltonian as[9]

$$H = \sum_{\boldsymbol{k}}[\epsilon(\boldsymbol{k})\Gamma^0 + A\sin(k_x)\Gamma^1 + A\sin(k_y)\Gamma^2 + M(\boldsymbol{k})\Gamma^5]c^\dagger_{\boldsymbol{k}}c_{\boldsymbol{k}}, \tag{3.12}$$

where $\Gamma^0 = I_{4\times4}$ and Γ^α, $\alpha = 1,\ldots,5$, form the Euclidean Clifford algebra $\Gamma^\mu\Gamma^\nu + \Gamma^\nu\Gamma^\mu = 2\delta^{\mu\nu}I_{4\times4}$. For this model we use the parameterizations $\Gamma^{(1,2,3,4,5)} = (\sigma^x\otimes s^z, -\sigma^y\otimes 1, \sigma^x\otimes s^x, \sigma^x\otimes s^y, \sigma^z\otimes 1)$, where both the σ's and s's are Pauli matrices acting on the s/p-like orbital space and the spin space $(\uparrow,\downarrow)$, respectively. Just like the preceding sections we want to calculate the energy spectrum and choose to make the y-direction finite with N_y lattice sites. Having lost the translational symmetry in this direction, k_y is no longer a good quantum number and we must Fourier transform it to lattice space. Introduce the Fourier transformation ($k \equiv k_x$)

$$c_{\boldsymbol{k}} = \frac{1}{L}\sum_{j=1}^{N_y} e^{ik_y j}c_{k,j},$$

in equation (3.12) and use $\frac{1}{L}\sum_{k_y} e^{ik_y(j'-j)} = \delta_{j,j'}$, $\sin k_y = \frac{e^{ik_y}-e^{-ik_y}}{2i}$ and $\cos k_y = \frac{e^{ik_y}+e^{-ik_y}}{2}$ to obtain

$$H = \sum_{k,j}\left(\mathscr{M}(k)c^\dagger_{k,j}c_{k,j} + \mathscr{T}c^\dagger_{k,j}c_{k,j+1} + \mathscr{T}^\dagger c^\dagger_{k,j+1}c_{k,j}\right), \tag{3.13}$$

$$\mathscr{M}(k) = [C - 2D(2-\cos k)]\Gamma^0 + A\sin k\Gamma^1 - 2B[2 - M/2B - \cos k]\Gamma^5, \tag{3.14}$$

$$\mathscr{T} = D\Gamma^0 + \frac{iA}{2}\Gamma^2 + B\Gamma^5. \tag{3.15}$$

In the following we will use the experimental values from König et al. [24], $A = 364.5\,\text{meV nm}a^{-1}$, $B = -686\,\text{meV nm}^2a^{-2}$, $C = 0$, $D = -512\,\text{meV nm}^2a^{-2}$, $M = -10\,\text{meV}$ and $a = 5\,\text{nm}$.

[7] One can also exploit the inversion symmetry and use the general formulation of the Z_2 number to understand the phase transitions. See Fu and Kane [13] for a readable account.

[8] This is just a fancy way of writing a combination of cross and scalar products.

[9] We will use the same symbol to denote the first and the second quantized operator as it introduces no confusion.

Energy spectrum, edge state wave functions and finite size effects

The Hamiltonian (3.13) is simpler than the Kane-Mele model on the honeycomb lattice and it can be diagonalized directly. The energy spectrum is shown in figure 3.4 for two different values of the topological mass M. As discussed earlier there is a energy gap for positive M characteristic for the topologically trivial insulator phase, while for negative M there are gapless edge states in the bulk gap. Rather than repeating the discussions from earlier, it is better

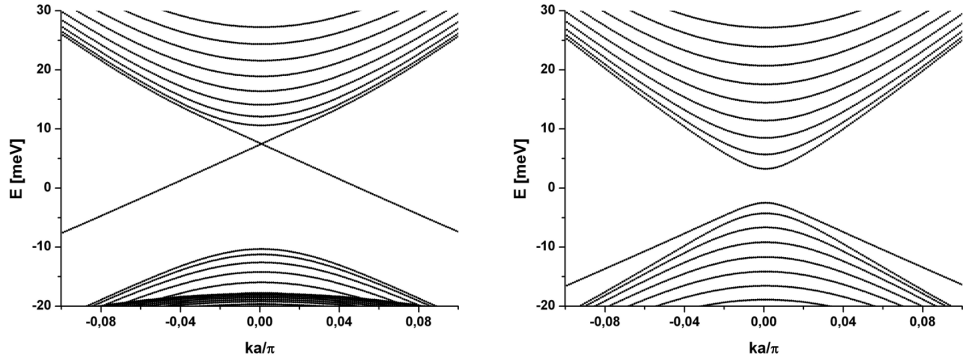

(a) $M = -10$ **(b)** $M = 2$

Figure 3.4: Energy spectrum for a large HgTe/CdTe quantum well sample for two different values of the topological mass M.

to show more directly why we use the terminology "gapless edge states", "bulk gap" and so on. The Hamiltonian (3.4) consists of a two-band spin-up part $h(\boldsymbol{k})$ and the time-reversed counterpart $h^*(-\boldsymbol{k}) = \Theta h(\boldsymbol{k})\Theta^{-1}$, where $\Theta = -i\sigma_y K$ is the time reversal operator and K stands for complex conjugation. The two sub-systems are uncoupled can be treated separately. Take a psudo-eigenspinor[10] for the upper block $h(\boldsymbol{k})\psi_\uparrow(\boldsymbol{k}) = E_{\boldsymbol{k}}\psi_\uparrow(\boldsymbol{k})$, where

$$\psi_\uparrow(\boldsymbol{k}) = \begin{pmatrix} \psi_{\uparrow+}(\boldsymbol{k}) \\ \psi_{\uparrow-}(\boldsymbol{k}) \end{pmatrix},$$

then it clear that for spin down part $h^*(-\boldsymbol{k})\psi_\downarrow(\boldsymbol{k}) = E_{\boldsymbol{k}}\psi_\downarrow(\boldsymbol{k})$, we must have $\psi_\downarrow(\boldsymbol{k}) = \Theta\psi_\uparrow(\boldsymbol{k})$. In figure 3.5, the probability distribution for spin up $|\psi_\uparrow(k,y)|^2 = |\psi_{\uparrow+}(k,y)|^2 + |\psi_{\uparrow-}(k,y)|^2$ and spin down $|\psi_\downarrow(k,y)|^2$ at a given energy is shown. On the left edge we have a counter propagating pair $\psi_\uparrow(k,y)$ and $\psi_\downarrow(-k,y)$, while on the other edge we have another pair with reversed propagation $\psi_\uparrow(-k,y)$ and $\psi_\downarrow(k,y)$. This verifies our claim, there are one counter propagating spin polarized pair on each edge in the energy range where the bulk is insulating. But as one can see in figure 3.5, for smaller sample size the wave functions overlap. It can generally be shown that backscattering is forbidden between time-reversed pairs in the QSH state, but finite size effects can overturn this. For example in figure 3.5b around $y = 0$ the spin up states on each edge overlap and this will definitely lead to backscattering since the fermions are counter propagating (and they are not time-reversed partners). This indicates that although time reversal symmetry is trying to keep the edge states gapless, a small gap may be induced due to finite size effects. This is indeed verified in figure 3.6, where the energy dispersion near the Dirac cone is shown. For $L = 800$ nm the cone is intact we have gapless edge states, but for $L = 200$ nm a small gap shown up with a magnitude of about $\Delta(L = 200\,\text{nm}) \approx 0.5$ meV

[10] Pseudo-spinor, since it describes pseudo-spin degree of freedom.

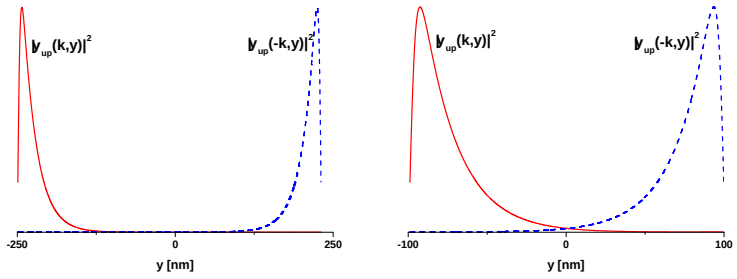

(a) Spin Up, $L = 500$ nm **(b)** Spin Up, $L = 200$ nm

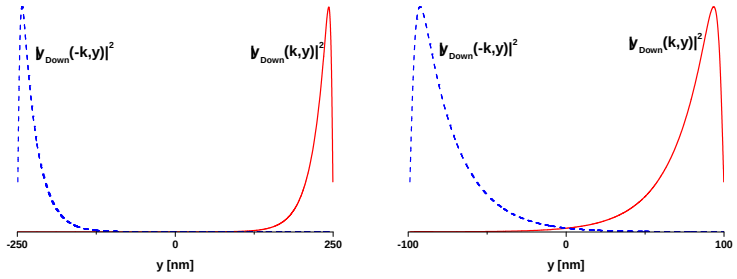

(c) Spin Down, $L = 500$ nm **(d)** Spin Down, $L = 500$ nm

Figure 3.5: Edge state probability distribution for $k = 0.01$, solid red line is for k and dashed blue line is for $-k$. It is seen that there is one counter propagating Kramer pair on each edge. For $L = 200$ nm the wave functions on each edge overlap due to finite size effects, this can lead to back scattering and a edge gap.

which might be measurable. These results are in agreement with the work of Zhou et al. [45].[11] These finite size effects might restrict the range of nano-scale applications of these HgTe/CdTe quantum wells. Linder et al. [29] has done a similar investigation on the surface states of the three-dimensional (Z_2) topological insulator and has found out that they show a remarkable robustness towards finite-size. Only when the sample size is about a few nanometers, a measurable gap shows up.

Another interesting feature of the time reversal invariant topological phases are that the edge states are believed to give rise to a quantized conductance $G = 2e^2/h$ and this has actually been observed experimentally. Furthermore these edge states are predicted to be insensitive to weak (time-reversal invariant) impurity scattering and even weak interactions. These properties are characteristic for these type of topological states of matter and it is therefore of our interest to investigate them further. To do this we need a machinery to perform non-equilibrium quantum transport calculations, which is the subject of the next chapter.

[11] Zhou et al. [45] uses the continuum model with the substitution $k_y \to -i\partial_y$ since k_y is not a good quantum number anymore. Then to solve the differential equations they use a trial functions of the form $e^{\lambda y}$ where $\lambda \in \mathbb{C}$. By a straightforward though very tedious calculation they end up with a semi-analytical solution.

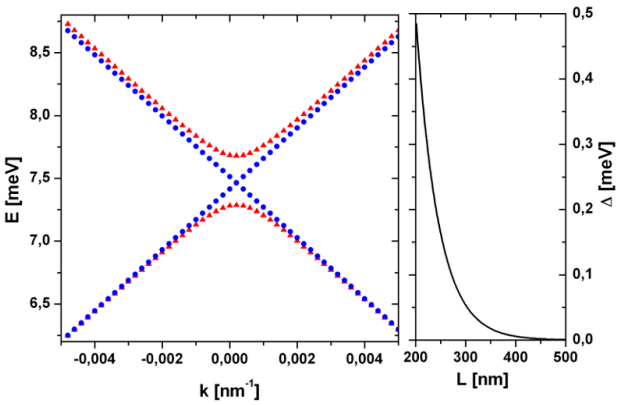

Figure 3.6: The figure to the left shows the energy spectrum near the Dirac cone, where the blue and red plots are for $L = 800$ nm and $L = 200$ nm, respectively. A energy gap emerges due to finite size effects. The figure on the right shows the gap as a function of the sample width, the gap opens up exponentially.

4 Keldysh formalism and non-equilibrium Green's functions

Contrary to a system in equilibrium, in non-equilibrium one cannot assume that the system returns to its ground state (or thermodynamic equilibrium at finite temperature) as time evolves. This means that in general the symmetry between $t = -\infty$ and $t = +\infty$, which is very important in the equilibrium theory, does not exist due to possible irreversible effects. In the case of non-equilibrium one can avoid this problem by allowing the system to evolve from the remote past, $t = -\infty$, to the moment of interest, $t = t_0$, and then continue back to $t = -\infty$. To be able to speak of time ordering one can define a contour in the complex plane, so a time τ_1 can be earlier than τ_2 on this contour even though their real-time projections may be of reversed order. Using this complex time contour allows one to treat the non-equilibrium problem in a similar fashion as in the equilibrium case, since all expectation values are defined with respect to a well defined state, i.e. the state which the system was in the remote past. There is though a price to pay, one has to treat the two time branches on an equal footing.

I have realized that giving an introduction to the non-equilibrium theory and sketch the proof of structural equivalence to the equilibrium theory is too time consuming. Since this is not a central part of this thesis, I will assume the reader is familiar with this formalism and knows about the analytic continuation rules (either Langreth theorem or the Keldysh approach). Uninitiated readers might want to look through the lecture notes [19, 40, 18][1] (which can be found on the Internet) or classical books on the subject (for example Meir and Wingreed or Haug and Jauho).

4.1 Non-equilibrium Quantum Transport

To study the robustness of the edge states on topological insulators against localized impurities, we need to calculate the steady-state current through the system. The formulas we are looking for in this section was first derived by Meir and Wingreen [31] and Jauho et al. [20], and we will more or less follow their approach.

The idea is quite simple, imagine that in the remote past the unperturbed system consists of three uncoupled regions: a left lead, a right lead and our sample of interest in the center. At $t = -\infty$ the three regions maintain their own thermal equilibrium and one can associate chemical potentials, μ_L and μ_R, to the left and right lead, respectively. Without loss of generality we shall assume that $\mu_L > \mu_R$. As the two leads are coupled to the sample, due to the

[1] The last reference is for people interested in the Functional Integral point of view. The notes are quit shallow, so it is recommended to start with Altland and Simons [1] for a good introduction to functional integrals in equilibrium.

difference in chemical potential, a current J starts to flow from the left to the right lead. After some initial transient effects, a steady state current emerges.

Define $c_\alpha^\dagger$ (c_α) to be the fermionic creation (annihilation) operator in the leads, where the index α includes all the relevant quantum numbers necessary to uniquely define a state in the leads. Taking the electrons to be non-interacting, we can write the Hamiltonian of both leads in a condensed notation as

$$H_{leads} = \sum_{\alpha \in L,R} \epsilon_\alpha c_\alpha^\dagger c_\alpha. \tag{4.1}$$

Since we are not investigating effects of interactions in topological insulators, we can similarly write the central region Hamiltonian as

$$H_{cen} = \sum_{n \in cen} \epsilon_n d_n^\dagger d_n, \tag{4.2}$$

where $d_n^\dagger$ (d_n) is the creation (annihilation) operator in the central region. In a real space lattice representation one can easily include impurities as on-site potentials through ϵ_n. Coupling these systems as discussed, will give rise to a tunneling term

$$H_T = \sum_{\substack{\alpha \in L,R \\ n \in cen}} \left(V_{\alpha,n} c_\alpha^\dagger d_n + h.c. \right) \tag{4.3}$$

and finally the total Hamiltonian may be written as $H = H_{leads} + H_{cen} + H_T$. Note however that we may have to assume that the leads are sufficiently large that they maintain their chemical potentials.

The average electric current from the left lead to the central region is defined as the average rate of change of particles times the electron charge

$$J = -e\langle \dot{N}_L \rangle, \tag{4.4}$$

where $N_L = \sum_{\alpha \in L} c_\alpha^\dagger c_\alpha$ is the occupation number operator of the left lead and the time evolution is with respect to H. The time derivative is given by

$$\dot{N}_L(t) = \frac{\mathrm{d}}{\mathrm{d}t}\left(e^{\frac{i}{\hbar}Ht} N_L e^{-\frac{i}{\hbar}Ht} \right) = \frac{i}{\hbar}[H, N_L](t) + (\partial_t N_L)(t),$$

and since H_{cen} and H_{leads} commutes with N_L we are left with

$$\begin{aligned} \dot{N}_L = \frac{i}{\hbar}[H_T, N_L] &= \frac{i}{\hbar} \sum_{\substack{\alpha \in L,R \\ n \in cen}} \sum_{\beta \in L} \left(\left\{ V_{\alpha,n} c_\alpha^\dagger d_n + V_{\alpha,n}^* d_n^\dagger c_\alpha \right\} c_\beta^\dagger c_\beta - c_\beta^\dagger c_\beta \left\{ V_{\alpha,n} c_\alpha^\dagger d_n + V_{\alpha,n}^* d_n^\dagger c_\alpha \right\} \right) \\ &= \frac{i}{\hbar} \sum_{\substack{\alpha \in L,R \\ n \in cen}} \sum_{\beta \in L} \left(V_{\alpha,n}[c_\alpha^\dagger, c_\beta^\dagger c_\beta] d_n + V_{\alpha,n}^* d_n^\dagger [c_\alpha, c_\beta^\dagger c_\beta] \right). \end{aligned} \tag{4.5}$$

Using the general formula $[C, AB] = \{A, C\}B - A\{B, C\}$ and the usual fermionic anti-commutator relations in equation (4.5), one can reduce equation (4.4) to

$$J_L = \frac{ie}{\hbar} \sum_{\substack{\alpha \in L \\ n \in cen}} \left(V_{\alpha,n} \langle c_\alpha^\dagger d_n \rangle - V_{\alpha,n}^* \langle d_n^\dagger c_\alpha \rangle \right) \tag{4.6}$$

One way to proceed is to express the averages in equation (4.6) in terms of Green's functions, since there exists several methods to calculate them. Looking at (4.6), it is natural to define the lesser Green's functions

$$G_{n,\alpha}^<(t, t') \equiv i\langle c_\alpha^\dagger(t') d_n(t) \rangle \tag{4.7}$$

$$G_{\alpha,n}^<(t, t') \equiv i\langle d_n^\dagger(t') c_\alpha(t) \rangle \tag{4.8}$$

with the useful property of the time diagonal elements $[G^<_{n,\alpha}(t,t)]^* = -G^<_{\alpha,n}(t,t)$. Inserting this in equation (4.6) we find the following expression for the current:[2]

$$J_L = \frac{e}{\hbar}\sum_{\substack{\alpha\in L\\ n\in cen}}\left(V_{\alpha,n}G^<_{n,\alpha}(t,t) - V^*_{\alpha,n}G^<_{\alpha,n}(t,t)\right) = \frac{e}{\hbar}\sum_{\substack{\alpha\in L\\ n\in cen}}\left(V_{\alpha,n}G^<_{n,\alpha}(t,t) + [V_{\alpha,n}G^<_{n,\alpha}(t,t)]^*\right)$$
$$= \frac{2e}{\hbar}\mathrm{Re}\Big\{\sum_{\substack{\alpha\in L\\ n\in cen}} V_{\alpha,n}G^<_{n,\alpha}(t,t)\Big\}. \tag{4.9}$$

In order to proceed we need an expression for $G^<_{n,\alpha}(t,t)$. If we are able to find an expression for the contour-ordered Green's function

$$G^C_{n,\alpha}(\tau,\tau') = -i\left\langle T_C\left\{d_n(\tau)c^\dagger_\alpha(\tau')\right\}\right\rangle, \tag{4.10}$$

an expression for $G^<_{n,\alpha}(t,t)$ can be found through analytical continuation rules. For this we can use that the non-equilibrium Green's functions have the same form as their $T=0$ equilibrium counterparts, so instead we consider the time-ordered equilibrium Green's function $G^t_{n,\alpha}(t,t') = -i\langle T_t\{d_n(t)c^\dagger_\alpha(t')\}\rangle$. Using the usual zero temperature equilibrium equation of motion technique (see [7, p. 140]) we arrive at[3]

$$-i\partial_{t'}G^t_{n,\alpha}(t-t') = \epsilon_\alpha G^t_{n,\alpha}(t-t') + \sum_{m\in cen} V^*_{\alpha,m}G^t_{n,m}(t-t'), \tag{4.11}$$

where $G^t_{n,m}(t-t') = -i\langle T_t\{d_n(t)d^\dagger_m(t')\}\rangle$. In case of no coupling between the leads and the central region we define the decoupled time ordered Green's function $g^t_\alpha(t_1,t') = -i\langle T_t\{c_\alpha(t_1)c^\dagger_\alpha(t')\}\rangle$ and again using the equation of motion technique we obtain

$$(i\partial_{t'} - \epsilon_\alpha)g^t_\alpha(t_1,t') = \delta(t_1-t'). \tag{4.12}$$

Multiplying equation (4.11) with $g^t_\alpha(t_1,t')$ and integrating with respect to t' gives

$$\int \mathrm{d}t'\left[-i\partial_{t'}G^t_{n,\alpha}(t,t')\right]g^t_\alpha(t_1,t') = \int \mathrm{d}t'\epsilon_\alpha G^t_{n,\alpha}(t,t')g^t_\alpha(t_1,t') \tag{4.13}$$
$$+\sum_m\int \mathrm{d}t' V^*_{\alpha,m}G^t_{n,m}(t,t')g^t_\alpha(t_1,t').$$

In order to make use of equation (4.11), we need to move the differentiation in the left hand side of equation (4.13) to $g^t_\alpha(t_1,t')$. So it is natural to integrate by parts

$$\int \mathrm{d}t'\left[-i\partial_{t'}G_{n,\alpha}(t,t')\right]g^t_\alpha(t_1,t') = -i\Big[G^t_{n,\alpha}(t,t')g^t_\alpha(t_1,t')\Big]^{t'=\infty}_{t'=-\infty} \tag{4.14}$$
$$+\int \mathrm{d}t' G^t_{n,\alpha}(t,t')\left[i\partial_{t'}g^t_\alpha(t_1,t')\right].$$

We must omit the first term since correlations on infinite time-scales are unphysical.[4] By inserting this into (4.13), making use of the δ-function in (4.12) and substituting $t_1 \leftrightarrow t'$ we find

$$G^t_{n,\alpha}(t,t') = \sum_m\int \mathrm{d}t_1 V^*_{\alpha,m}G^t_{n,m}(t,t_1)g^t_\alpha(t_1,t'). \tag{4.15}$$

[2] It might appear as if the average current is suddenly time dependent, but in steady state only time differences matter. This means that $G^<_{n,\alpha}(t,t') = G^<_{n,\alpha}(t-t') \Rightarrow G^<_{n,\alpha}(t,t) = G^<_{n,\alpha}(0,0) = i\langle c^\dagger_\alpha d_n\rangle$.

[3] This is basically a matter of differentiating and using the relevant (anti-)commutator relations.

[4] I must admit that this is not so rigorous, but I think that this requirement should be imposed as a boundary condition on physical grounds. Meir and Wingreen [31] and [20] do this differently and do not have this problem, but I have failed in understanding their method.

We are now able to exploit the structural equivalence between the equilibrium and non-equilibrium theory by changing the integration to be along the Keldysh contour

$$G^C_{n,\alpha}(\tau,\tau') = \sum_m \int_C \mathrm{d}\tau_1 V^*_{\alpha,m} G^C_{n,m}(\tau,\tau_1) g^C_\alpha(\tau_1,\tau'). \tag{4.16}$$

According to the analytical continuation rules we obtain [19, 40, 18]

$$G^<_{n,\alpha}(t,t') = \sum_m \int \mathrm{d}t_1 V^*_{\alpha,m} \left[G^R_{n,m}(t,t_1) g^<_\alpha(t_1,t') + G^<_{n,m}(t,t_1) g^a_\alpha(t_1,t') \right], \tag{4.17}$$

where the superscripts R and a stands for the usual retarded and advanced greens functions, respectively. Using that only time difference matters (in steady state) and the convolution theorem for Fourier transforms, the average current may now be expressed as[5]

$$J_L = \frac{2e}{\hbar} \sum_{\substack{\alpha\in L \\ n,m}} \int \frac{\mathrm{d}\omega}{2\pi} \mathrm{Re}\Big\{ V^*_{\alpha,m} V_{\alpha,n} \left[G^R_{n,m}(\omega) g^<_\alpha(\omega) + G^<_{n,m}(\omega) g^a_\alpha(\omega) \right] \Big\}. \tag{4.18}$$

Now note that[6] $g^<_\alpha(t-t') = i\langle c^\dagger_\alpha c_\alpha\rangle e^{-i\epsilon_\alpha(t-t')} = i f_L(\epsilon_\alpha) e^{-i\epsilon_\alpha(t-t')}$ and similarly $g^a_\alpha(t-t') = i\theta(t'-t)e^{-i\epsilon_\alpha(t-t')}$, where $f_L(\epsilon_\alpha)$ is the fermi-distribution for the left lead. By putting the α summation and the V's inside the line-width function $\Gamma_{m,n}(\omega)$ we find after a straightforward but tedious manipulation

$$J_L = \frac{e}{h} \int \mathrm{d}\omega [f_L(\omega) - f_R(\omega)] \mathrm{Tr}\left\{ \boldsymbol{G}^a \boldsymbol{\Gamma}_R \boldsymbol{G}^r \boldsymbol{\Gamma}_L \right\}, \tag{4.19}$$

where we have used matrix notation instead of the n, m summations and used that in steady state $J = J_L = -J_R = (J_L - J_R)/2$. In the limit $T \to 0$, $f_L(\omega)$ and $f_R(\omega)$ are step functions, and to linear order in $\mu_L - \mu_R$ we find

$$J_L = \frac{e}{h} \mathrm{Tr}\left\{ \boldsymbol{G}^a \boldsymbol{\Gamma}_R \boldsymbol{G}^r \boldsymbol{\Gamma}_L \right\} (\mu_L - \mu_R) = \frac{e^2}{h} \mathrm{Tr}\left\{ \boldsymbol{G}^a \boldsymbol{\Gamma}_L \boldsymbol{G}^r \boldsymbol{\Gamma}_R \right\} (V_L - V_R). \tag{4.20}$$

Finally the linear conductance is then given by

$$G = J_L/(V_L - V_R) = \frac{e^2}{h} \mathrm{Tr}\left\{ \boldsymbol{G}^a \boldsymbol{\Gamma}_R \boldsymbol{G}^r \boldsymbol{\Gamma}_L \right\}. \tag{4.21}$$

It is assumed that the spin is included in the n, m summations or else a factor of two is necessary.

4.2 Self-energies

In studying the effects of disorder on the electronic state of HgTe/CdTe QW's, we will model the two leads as semi-infinite clean copies of the HgTe/CdTe sample. This introduces some difficulties since semi-infinite leads will inevitably make the total Hilbert space (and thereby Hamiltonian) infinite-dimensional. This problem can however be solved. The retarded Green's function of the central region can be calculated by, loosely speaking, renormalizing the contribution of the leads into self energies and adding them to the central region Hamiltonian. This

[5] The factor $e^{i\omega(t-t')}$ is not present since $t = t'$.

[6] Recall that these are Green's functions in the isolated lead, thus the time-evolution and average is with respect to the left lead Hamiltonian only.

may be regarded as the effective Hamiltonian of the system, although it will not be hermitian in general.[7]

The central region retarded Greens function is given by, [8, 9, 44]

$$\boldsymbol{G}^r_{cen} = (E\boldsymbol{I} - \boldsymbol{H}_{cen} - \boldsymbol{\Sigma}_L - \boldsymbol{\Sigma}_R)^{-1}, \tag{4.22}$$

where $\boldsymbol{H}_{cen}$ is the Hamiltonian matrix of the decoupled central region, and $\boldsymbol{\Sigma}_{[L,R]}$ are the self-energy terms due to the coupling with the leads. The self-energies can be expressed as

$$\begin{aligned} \boldsymbol{\Sigma_L} &= \boldsymbol{H}^\dagger_{LC}\boldsymbol{g}_L\boldsymbol{H}_{LC}, \\ \boldsymbol{\Sigma_R} &= \boldsymbol{H}_{CR}\boldsymbol{g}_R\boldsymbol{H}^\dagger_{CR}, \end{aligned} \tag{4.23}$$

where $\boldsymbol{H}_{LC}$ and $\boldsymbol{H}_{CR}$ are the coupling matrices that are nonzero only for adjacent points in the central region. The matrices $\boldsymbol{g}_L$ and $\boldsymbol{g}_R$ are the surface Green's functions of the left and right lead, respectively. The surface Green's functions are to be understood as sub-blocks of the semi-infinite leads' retarded Green's functions (infinite dimensional matrix). Finally the matrices $\boldsymbol{\Gamma}_{[L,R]}$ are related to the self energies by [8, 9]

$$\boldsymbol{\Gamma}_{[L,R]} = i\left[\boldsymbol{\Sigma}_{[L,R]} - \boldsymbol{\Sigma}^\dagger_{[L,R]}\right].$$

Clearly the key issue is how to calculate $\boldsymbol{g}_L$ and $\boldsymbol{g}_R$, since getting them from the full Green's function would involve inverting infinite dimensional matrices.

In the literature many different numerical methods exits for this purpose, with the so called recursive Green's function method, being the most popular. However we will use the method developed by Lee and Joannopoulos [27] since it is both faster and easier to implement than the usual recursive algorithm. Although the authors developed this method for surface-band calculations, a small modification makes it also useful for transport problems [44].[8] We briefly summarize this scheme, for detailed derivation see [27].

Surface Green's functions of semi-infinite leads

In the following we will concentrate on the right lead. Consider a semi-infinite two dimensional system and assume that it can be described by localized orbitals on a lattice. Now decompose the leads into a semi-infinite stack of principal layers, where a principal layer is the smallest group of neighboring atomic layers such that only nearest-neighbor interactions between principal layers exist. We will restrict ourself to systems with only one type of principal layers, although it is no difficult to generalize to more complicated situations. Assume that each principal layer has μ lattice points and let $\phi_\alpha(l)$ be an orbital in the l'th principal layer[9]. The Hamiltonian can then be written in a block-matrix form

$$\boldsymbol{H} = \begin{pmatrix} \boldsymbol{H}_{00} & \boldsymbol{H}_{01} & 0 & \dots \\ \boldsymbol{H}_{10} & \boldsymbol{H}_{11} & \boldsymbol{H}_{12} & \\ 0 & \boldsymbol{H}_{21} & \boldsymbol{H}_{22} & \ddots \\ \vdots & & \ddots & \ddots \end{pmatrix} \tag{4.24}$$

[7] Actually the conductance will vanish if the self energies are hermitian.

[8] This method can also straightforwardly be used to calculate LDOS of 3D topological insulator surfaces, useful for explaining STM experiments.

[9] Each lattice site may of course contain several bands, as is the case with our HgTe/CdTe sample. In such situations, $\phi_\alpha(l)$ can be thought of as a spinor.

where each sub-block, $\boldsymbol{H}_{ll'}$, is given by

$$[\boldsymbol{H}_{ll'}]_{\alpha\beta} = \langle\phi_\alpha(l)|\boldsymbol{H}|\phi_\beta(l')\rangle$$

for $\alpha,\beta = 1,2,\ldots,\mu$ and $l,l' = 0,1,\ldots,\infty$. In this picture $\boldsymbol{H}_{ll}$ describes the l'th principal layer while $\boldsymbol{H}_{ll+1}$ and $\boldsymbol{H}_{l+1l}$ describes the interactions with the nearest neighbors. The matrix elements of the Green's function are given by[10]

$$[G_{ll'}(E^+)]_{\alpha\beta} = \langle\phi_\alpha(l)|(E^+ - \boldsymbol{H})^{-1}|\phi_\beta(l')\rangle, \tag{4.25}$$

where $E^+ = E + i\eta$ and η is an infinitesimal positive number. Since we have chosen the zeroth principal layer as the surface of the semi-infinite lead, $\boldsymbol{G}_{00}$ is the surface Green's function we are looking for. Looking at $(E^+ - \boldsymbol{H})\boldsymbol{G} = \boldsymbol{I}$ in the basis of equation (4.25), it is easy to see that only the first column couples to $\boldsymbol{G}_{00}$. Thus the set of matrices $\{\boldsymbol{G}_{l0}; 0 \le l < \infty\}$ must satisfy

$$\begin{pmatrix} (E^+ - \boldsymbol{H}_{00}) & -\boldsymbol{H}_{01} & \boldsymbol{0} & \cdots \\ -\boldsymbol{H}_{01}^\dagger & (E^+ - \boldsymbol{H}_{00}) & -\boldsymbol{H}_{01} & \\ \boldsymbol{0} & -\boldsymbol{H}_{01}^\dagger & (E^+ - \boldsymbol{H}_{00}) & -\boldsymbol{H}_{01} \\ \vdots & \boldsymbol{0} & -\boldsymbol{H}_{01}^\dagger & \ddots \end{pmatrix} \begin{pmatrix} \boldsymbol{G}_{00} \\ \boldsymbol{G}_{10} \\ \boldsymbol{G}_{20} \\ \vdots \end{pmatrix} = \begin{pmatrix} \boldsymbol{I} \\ \boldsymbol{0} \\ \boldsymbol{0} \\ \vdots \end{pmatrix} \tag{4.26}$$

where we have used that only one inequivalent principal layer is considered. Meaning that $\boldsymbol{H}_{00} = \boldsymbol{H}_{ll}$, $\boldsymbol{H}_{01} = \boldsymbol{H}_{ll+1}$ and $\boldsymbol{H}_{l+1l} = \boldsymbol{H}_{ll+1}^\dagger$ for $0 \le l < \infty$. Now define the transfer matrix as follows:

$$\boldsymbol{T}(E^+) = \begin{pmatrix} \boldsymbol{H}_{01}^{-1}(E^+ - \boldsymbol{H}_{00}) & -\boldsymbol{H}_{00}^{-1}\boldsymbol{H}_{01}^\dagger \\ \boldsymbol{I} & \boldsymbol{0} \end{pmatrix}, \tag{4.27}$$

it is straightforward to see that

$$\begin{pmatrix} \boldsymbol{G}_{(n+1)0} \\ \boldsymbol{G}_{n0} \end{pmatrix} = \boldsymbol{T}^n \begin{pmatrix} \boldsymbol{G}_{10} \\ \boldsymbol{G}_{00} \end{pmatrix}. \tag{4.28}$$

Lee and Joannopoulos [27] proves that the outcome by affiliating an infinitesimal positive imaginary part with E is that half of the eigenvalues of the $2\mu \times 2\mu$ matrices $\boldsymbol{T}(E^+)$ have modulus less than 1 and half have modulus greater than 1. Let us assume that $|\lambda_\beta| < 1$ when $1 \le \beta \le \mu$ and $|\lambda_\beta| > 1$ when $\mu + 1 \le \beta \le 2\mu$.

Equation (4.28) shows that the transfer matrix somehow contains information about the Green's functions on each principal layer and the main idea is that we want to express the surface Green's function in terms of the eigenvectors of $\boldsymbol{T}(E^+)$. In order for the surface Green's function to satisfy (4.28) and remain normalizable, one must only retain the eigenvalues $|\lambda_\beta| < 1$. This implies that $\begin{pmatrix} \boldsymbol{G}_{(n+1)0} \\ \boldsymbol{G}_{n0} \end{pmatrix}$ can be expanded in terms of the eigenvectors $\boldsymbol{e}_\beta(E^+)$ with $1 \le \lambda_\beta \le \mu$. In particular, we may write

$$\begin{pmatrix} \boldsymbol{G}_{10} \\ \boldsymbol{G}_{00} \end{pmatrix} = \begin{pmatrix} \boldsymbol{S}_2\mathscr{G}_1 \\ \boldsymbol{S}_1\mathscr{G}_1 \end{pmatrix}$$

with

$$(\boldsymbol{S}_1)_{\alpha\gamma} = \boldsymbol{v}_\alpha \cdot \boldsymbol{e}_\gamma,$$
$$(\boldsymbol{S}_2)_{\alpha\gamma} = \boldsymbol{u}_\alpha \cdot \boldsymbol{e}_\gamma,$$

[10] Recall the definition $(E^+ - \boldsymbol{H})\boldsymbol{G} = \boldsymbol{I}$. Multiplication with identity matrices of correct size is implied.

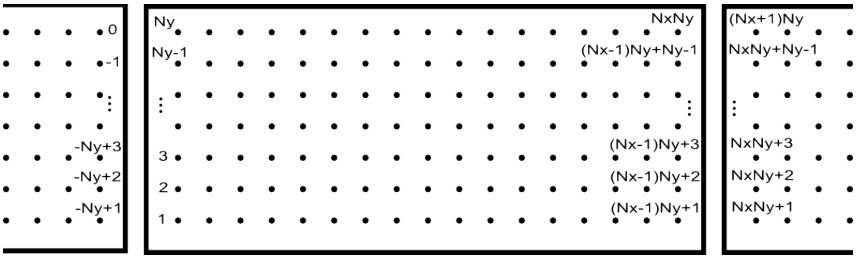

Figure 4.1: A more convenient way of numbering the lattice sites. The left lead corresponds to $m = -\infty,\ldots,0$, the central region $m = 1,\ldots,N_xN_y$ and the right lead $m = N_xN_y+1,\ldots,\infty$.

where $\alpha,\gamma = 1,2,\ldots,\mu$, $\boldsymbol{u}_\alpha$ and $\boldsymbol{v}_\alpha$ are 2μ-dimensional column vectors with components given by $(\boldsymbol{u}_\alpha)_i = \delta_{\alpha,i}$ and $(\boldsymbol{v}_\alpha)_i = \delta_{\alpha+\mu,i}$. The matrix $\mathscr{G}_1$ represents the unknown expansion coefficients, while the eigenvectors with eigenvalues $\lambda_\beta < 1$ are represented by $\boldsymbol{S}_1$ and $\boldsymbol{S}_2$. Finally it can be shown that the surface Green's function $\boldsymbol{g}_R$ (= $\boldsymbol{G}_{00}$) is given by

$$\boldsymbol{g}_R = \left[(E^+ - \boldsymbol{H}_{00}) - \boldsymbol{H}_{01}\boldsymbol{S}_2\boldsymbol{S}_1^{-1}\right]^{-1}. \tag{4.29}$$

To obtain the surface Green's function of the left lead one has to make the substitution $\boldsymbol{H}_{01} \rightarrow \boldsymbol{H}_{10}$ in equation (4.27) and (4.29), since the surface is along the other end.

The HgTe/CdTe Hamiltonian

All in all one needs the $\boldsymbol{H}_{00}$ and H_{01} matrices to calculate the surface Green's functions of the leads, then afterwards the central region Hamiltonian matrix plus the coupling matrices to calculate the central region retarded Green's function. Having found all that, equation (4.21) finally gives the linear conductance. In order to obtain the needed matrices for our system of interest we have to introduce the Fourier transform

$$c_{\boldsymbol{k}} = \frac{1}{\Omega}\sum_{ij} e^{i\boldsymbol{k}\cdot\boldsymbol{R}} c_{\boldsymbol{R}},$$

in equation (3.12), where $\boldsymbol{R} = (i,j)$, to get the Hamiltonian

$$H = \sum_{ij}\left(\mathscr{M}c_{ij}^\dagger c_{ij} + \mathscr{T}_y c_{ij}^\dagger c_{ij+1} + \mathscr{T}_y^\dagger c_{ij+1}^\dagger c_{ij} + \mathscr{T}_x c_{ij}^\dagger c_{i+1j} + \mathscr{T}_x^\dagger c_{i+1j}^\dagger c_{ij}\right), \tag{4.30}$$

$$\mathscr{M} = [C-4D]\,\Gamma^0 + [M-4B]\,\Gamma^5, \tag{4.31}$$

$$\mathscr{T}_y = D\Gamma^0 + \frac{iA}{2}\Gamma^2 + B\Gamma^5, \tag{4.32}$$

$$\mathscr{T}_x = D\Gamma^0 + \frac{iA}{2}\Gamma^1 + B\Gamma^5, \tag{4.33}$$

where the sum is over all the sites. This may be written in the form $H = \sum_{ij} H_{ii'jj'}c_{ij}^\dagger c_{i'j'}$ with

$$H_{ii'jj'} = \mathscr{M}\delta_{ii'}\delta_{jj'} + \mathscr{T}_y\delta_{ii'}\delta_{j+1j'} + \mathscr{T}_y^\dagger\delta_{ii'}\delta_{jj'+1} + \mathscr{T}_x\delta_{i+1i'}\delta_{jj'} + \mathscr{T}_x^\dagger\delta_{ii'+1}\delta_{jj'}. \tag{4.34}$$

Taking the leads to be along the x-direction, the blocks in the matrix (4.24) is constructed by defining $(\boldsymbol{H}_{ii'})_{jj'} = H_{ii'jj'}$. In particular $(\boldsymbol{H}_{00})_{jj'} = \mathscr{M}\delta_{jj'} + \mathscr{T}_y\delta_{j+1j'} + \mathscr{T}_y^\dagger\delta_{jj'+1}$, $(\boldsymbol{H}_{01})_{jj'} =$

$\mathscr{T}_x\delta_{jj'}$ and $\boldsymbol{H}_{10} = \boldsymbol{H}_{01}^\dagger$ or in matrix form

$$\boldsymbol{H}_{00} = \begin{pmatrix} \mathscr{M} & \mathscr{T}_y & & \\ \mathscr{T}_y^\dagger & \mathscr{M} & \ddots & \\ & \ddots & \ddots & \mathscr{T}_y \\ & & \mathscr{T}_y^\dagger & \mathscr{M} \end{pmatrix} \qquad \boldsymbol{H}_{01} = \begin{pmatrix} \mathscr{T}_x & & & \\ & \ddots & & \\ & & \ddots & \\ & & & \mathscr{T}_x \end{pmatrix}, \tag{4.35}$$

where both matrices are $4N_y \times 4N_y$.

Next we need to find the central region Hamiltonian which consists of the clean part (4.30) and a part with randomly distributed impurities. It is convenient to reduce the two indices $i = 1,\ldots,N_x,\ j = 1,\ldots,N_y$ into one $m = 1,\ldots,N_xN_y$, by the change of basis shown in figure 4.1.[11] Thus $H_{\text{cen}} = \sum_{m,m'=1}^{N_xN_y} h_{mm'}c_m^\dagger c_{m'}$ with

$$(\boldsymbol{H}_{\text{cen}})_{mm'} \equiv h_{mm'} = (\mathscr{M} + W_m)\,\delta_{mm'} + \mathscr{T}_y\delta_{m+1m'} + \mathscr{T}_y^\dagger\delta_{mm'+1} + \mathscr{T}_x\delta_{m+N_ym'} + \mathscr{T}_x^\dagger\delta_{mm'+N_y}, \tag{4.36}$$

which is a $4N_xN_y \times 4N_xN_y$ matrix. Here W_m is the on-site impurity potential

$$W_m = \begin{pmatrix} W_{\uparrow+,m} & & & \\ & W_{\uparrow-,m} & & \\ & & W_{\downarrow+,m} & \\ & & & W_{\downarrow-,m} \end{pmatrix},$$

where the coefficients are disorder energies uniformly distributed in the range $[-\frac{W}{2}, \frac{W}{2}]$, for non-magnetic impurities we have $W_{\uparrow+,m} = W_{\downarrow+,m}$ and $W_{\uparrow-,m} = W_{\downarrow-,m}$. Finally by looking at figure 4.1 one can see that the tunneling between the leads and the central region is given by[12]

$$H_{L\leftrightarrow C} + H_{R\leftrightarrow C} = \sum_{m=1}^{N_xN_y}\sum_{m'=-N_x+1}^{0}\left(\mathscr{T}_x^\dagger\delta_{m,m'+N_y}c_m^\dagger c_{m'} + h.c.\right) + \sum_{m=1}^{N_xN_y}\sum_{m'=N_xN_y+1}^{(N_x+1)N_y}\left(\mathscr{T}_x\delta_{m+N_ym'}c_m^\dagger c_{m'} + h.c.\right), \tag{4.37}$$

which is written in a form easy to implement.

4.3 Numerical implementation

By looking at the steps involved in implementing this calculation, it appears to be a very simple and straightforward task. And indeed it is. But one quickly realizes that even for very small systems, say a 30×20 lattice, calculating the conductance just one time is almost impossible even for a rather fast modern computer. But we are interested in calculating the conductance for, say 100 different values of W, using much bigger systems and averaging several hundred times for each fixed W. Other authors, for example [21], have had access to huge clusters with several hundred processors and many gigabytes of ram. It is therefore impossible to do anything useful with a naive implementation. The single most challenging and time consuming

[11] In this representation we only need one set of annihilation c_m and creation $c_m^\dagger$ operators.

[12] We have to use $\mathscr{T}_x$ since the leads are connected to the central region only in this direction. The sum has to be over all sites in the central region but only over the surface sites of the leads to get the correct sized matrices (see equation (4.23)), off course only the coupling between the surfaces are non-zero. Whether to use $\mathscr{T}_x$ or $\mathscr{T}_x^\dagger$ depends on which way the fermions "jump".

part of this project was to optimize the code.[13] A detailed account of what was done is beyond the time and space limit of this work, but I will mention a few of the most important aspects.

Three 64 bit computers, each with 8 cores ~ 3 GHz and 2 Gigabytes of RAM, were available. The strategy was to make use of multi-threaded programming in well-chosen places and keep the RAM usage low.[14] First of all, in equation (4.22) we have to invert some huge matrices. Using a 200×80 lattice, the size of the matrices will be $4N_xN_y \times 4N_xN_y = 64.000 \times 64.000$ which is impossible even if we had much more RAM available.[15] A simple analysis reveals that in equation (4.21) only the upper right $4N_y \times 4N_y$ sub-block of the Green's function is needed and not the whole matrix. For this part the algorithm proposed by Drouvelis et al. [10] was used, but with some small modifications (be aware of some crucial misprints in their paper). This algorithm reduces the numerical complexity from about $(4N_xN_y)^3$ to about $7N_xN_y^3$ for a single processor (and even more if the multi-threaded version is utilized).

Another problem is that just writing for example $\boldsymbol{H}_{cen}$ once for a 200×80 lattice without any calculation, takes more than one minute. Since we need to average over many systems of randomly distributed impurities, only this (almost trivial) operation will take several weeks to accomplish. Furthermore it eats up all the RAM. The way to solve this problem is to rewrite this, and many other matrices, as sparse matrices and thereby make these operations ridiculously fast with almost no RAM usage.[16] Other type of problems are matrix multiplications which also have a N^3 numerical complexity. For example the multiplication in equation (4.23) can be made much faster and more RAM friendly by noticing that due to the form of the coupling matrices, only a few elements end up being non-zero. So by some clever tricks, this sort of problems are easily solved.

Parallel programming is used many different but strategically chosen places, for example while calculating the self energies and averaging over different random configurations. Instead of averaging uniformly as a function of W, a special function has been constructed to average more when it is needed and less when it is not. This function has some parameters which can be used to adjust the profile to meet ones needs. A final thing worth mentioning is that in order to calculate local density of states, another part of the Greens functions are needed. The algorithm proposed by Drouvelis et al. [10] will not be useful anymore. For this I have used a modified version of the algorithm proposed by Godfrin [14].

All this hard work does not only make this calculation possible to perform, but it also makes it more environmental friendly. Who knows, maybe this sacrifice will be the reason why the earth and humanity survives in the end?

[13] Well, another time consuming task was to find an apparently invisible bug in the code. After a month of stagnation it turned out to be a small misprint in an article and not the code.

[14] Mainly because the RAM is one the few weaknesses of the computers available and by using 8 threads on each computer, the ram usage gets 8 times bigger.

[15] Note that although $E\boldsymbol{I} - \boldsymbol{H}_{\text{cen}} - \boldsymbol{\Sigma}_L - \boldsymbol{\Sigma}_R$ is sparse, the inverse will we a dense matrix in general.

[16] The transfer matrices should not be converted to sparse matrices, since eigenvalue/vector algorithms for dense matrices are much faster for large matrix size.

5 Topological Anderson Insulator

We are now able to perform non-equilibrium quantum transport calculations to see whether the conductance of the edge states is quantized in exact units of $2e^2/h$ and whether this quantization is insensitive to weak non-magnetic impurities. To summarize, we have a two-dimensional HgTe/CdTe system with $N_x \times N_y$ lattice sites which is connected to two leads with different chemical potentials. The leads are modeled as two semi-infinite clean copies of the HgTe/CdTe sample, while non-magnetic impurities are spread randomly on the central region. The impurities are taken to be simple on-site potentials with energies in the range $[-\frac{W}{2}, \frac{W}{2}]$, spread according to the uniform distribution. This setup is widely used in the Anderson localization literature.

5.1 Results of transport calculations

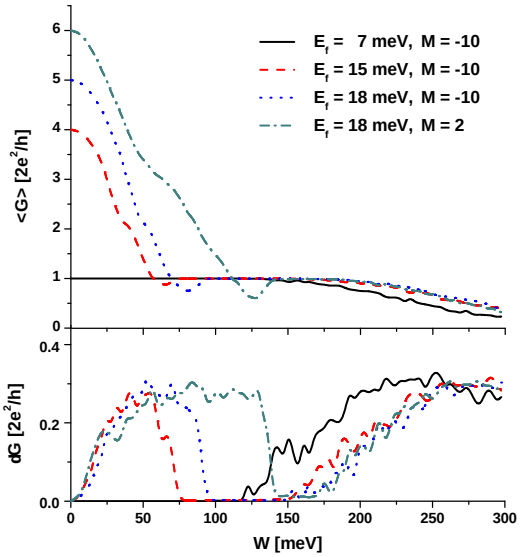

Figure 5.1: The average conductance $\langle G \rangle$ and standard deviation δG as a function of the disorder potential W for different values of the Fermi energy E_f. The lattice size is 200×80 and there have been averaged over up to 180 random configurations.

In figure 5.1 the average conductance $\langle G \rangle$ and fluctuations δG as a function of the disorder potential W is shown for different values of the Fermi energy E_f. It is recommendable to take a look at the energy spectrum in figure 3.4 to understand where the Fermi level lies. As predicted, when the sample is in the QSH state ($M = -10$) and the Fermi energy in the bulk

gap ($E_f = 7$) the conductance is exactly $G = 2e^2/h$. This is due to a spin up and one spin down current on opposite edges, each contributing with e^2/h.[1] As the Fermi energy is raised above the bulk gap, the conductance naturally grows since the bulk channels are also conducting (for $W = 0$).

When impurities are introduced the remarkable topological stability of the edge states ($E_f = 7$) are seen, the conductance remains perfectly quantized for a large range of W. Only above a high level of impurities, the conductance begins to fall and the edge states become localized. This property is a key signature for experimental identification of the QSH phase. It is also worth noticing that the standard deviation is identically zero while the conductance is quantized, and only at large W, fluctuations are observed. This means that the edge states remain insensitive for any impurity configuration and not only on average. Of course this is a clear sign that no scattering occurs and the edge flow is dissipationless. For all Fermi energies in the bulk gap there is no qualitative change of this behavior.

For energies above the bulk gap the conductance falls due to impurity scattering, which is expected. Highly surprising at a critical W_c (which clearly depends on E_f) the conductances are getting quantized with $G = 2e^2/h$, where usually Anderson localization is observed. Furthermore as long as this quantization maintains, the fluctuations are identically zero. This resembles the case with the Fermi energy lying the in bulk gap and with some courage one may postulate that topologically robust edge states have emerged due to impurities. Even more surprising, when $M = 2$, and the HgTe/CdTe QW is in the trivial insulating state, the exact same phenomenon is seen. Remember that for $M = 2$ ($W = 0$) there are no topological effects, even when the Fermi energy lies in the bulk gap (see figure 3.4) and seeing these effects emerge due to impurities are more surprising than in the $M = -10$ case. It is natural to suspect that at this critical W_c a topological phase transition occurs. Another puzzling aspect is that when the Fermi energy is below the bulk gap, nothing interesting happens other than Anderson localization (not shown on the figures). These surprising effects were recently discovered by Li et al. [28] in numerical simulations similar to ours and later verified by Jiang et al. [21] by a new set of simulations. Li et al. [28] baptized the phase as *Topological Anderson Insulator*.[2]

Of course the question remains, does this conductance quantization have anything to do with edge states? To answer this question the average conductance has been calculated for different sample width $L_y = aN_y$ at a fixed Fermi energy ($E_f = 15$). In figure 5.2 this is shown for $M = -10$ (left figure) and $M = 2$ (right figure). For no impurities the conductance grows for larger sample width, since more conducting channels become available (for $E_f = 15$, the sample is conducting). When W is increased a phase transition occurs at a critical W_c to the TAI state, the conductance is $G = 2e^2/h$ with $\delta G = 0$ and W_c does not depend on the sample size. This indicates that when the system is in the TAI state the conducting channels might be living near the sample edge, if the bulk was conducting the conductance should grow for larger width.[3] For $M = 2$ the same thing happens, but although W_c is independent of the length it clearly depends on M.

A way to see were these conducting states are localized is by calculating the local density of states (LDOS), which is given by the usual formula $\rho(y) = -\frac{1}{\pi}\frac{1}{N_x}\sum_{x=1}^{N_x} G(x,y)$, here we have

[1] When the system is in non-equilibrium, the states propagating in the other direction are not occupied.

[2] Our simulations are in great agreement with other similar works.

[3] Of course, this is not a proof. The conducting channel could as well be in the middle of the sample. Or maybe the whole bulk is conducting but the current is redistributed as the width is increased, such that the overall conductance is quantized and unchanged.

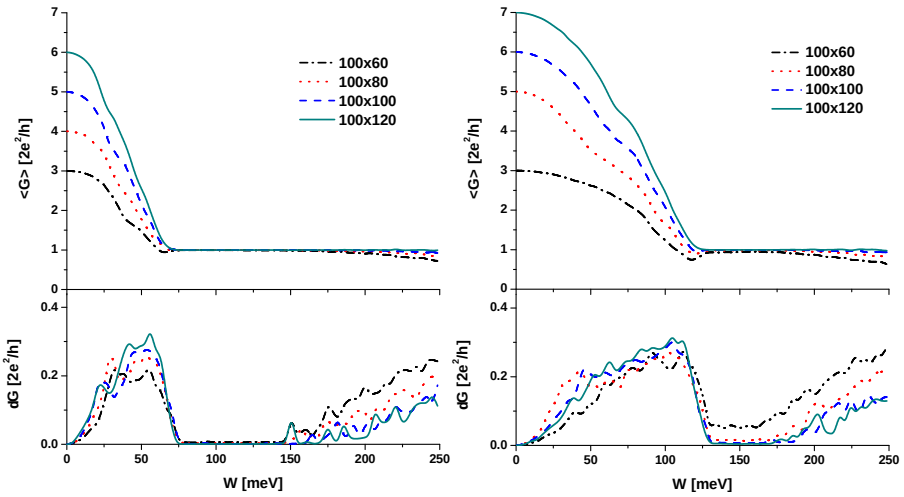

Figure 5.2: The average conductance $\langle G \rangle$ and standard deviation δG as a function of the disorder potential W for different sample width $L_y = aN_y$. The Fermi energy is fixed at $E_f = 15$ and there have been averaged over up to 150 random configurations. The left figure is for $M = -10$ and the right for $M = 2$.

average over the sites in the x-direction.[4] This is shown in figure 5.3 for a 200×80 lattice with $M = -10$, but for different values of E_f and W. As expected, in the case with no impurities and the Fermi level lying in the bulk gap ($E_f = 7$), states are only present along the edges of the sample while the bulk is insulating. When the Fermi energy is raised to $E_f = 15$, states become available in the bulk since we are in the conduction band. Now impurities are introduced with $W = 50$, such that the system is not in the TAI state (see figure 5.1). The bulk states seem to be affected by the impurities, again expected. We are not averaging over different impurity configurations so calculating ρ twice for $W = 50$ gives two different results due to fluctuations, but nothing changes qualitatively. Finally when $W = 100$ and we are in the TAI state, the bulk states are gone while only edge states are present. No fluctuation are seen when this is calculated for different impurity configurations, in agreement with figure 5.1.

In order to convince the reader even more we have implemented local current calculations into our program, but due to lack of computational power we are unable to perform these calculations for big enough lattices such that TAI state is seen clearly.[5] Jiang et al. [21] have done similar calculations and we have borrowed some of their figures, only the spin up subsystem is shown. They use the same setup as us except that they only put impurities in a region in the middle of the sample, furthermore they average 500 times since they have access to more computational power. In figure 5.4 (left) the system is in the QSH state and it is seen that current is only non-zero along the upper edge (spin down along the lower edge). As long as the system remains is this phase (see figure 5.1) the edge states are preserved. In figure

[4] Here we are in the equilibrium situation (no leads present). The Green's function in equilibrium is given by $\boldsymbol{G} = \left[(E + i\eta)\boldsymbol{I} - \boldsymbol{H}_{cen}\right]^{-1}$, and $G(x, y)$ is then given by the diagonal elements of $\boldsymbol{G}$. Since this is written in the basis shown in figure 4.1, one has to construct a simple function translating between the lattice coordinates (x, y) and m.

[5] Local current calculations require the whole central region Green's function and as described earlier this is impossible to calculate directly for large systems unless a huge cluster is available. But I have some ideas which might make this task possible to perform, but it requires too much time to implement and test through. Maybe this will be implemented in the future.

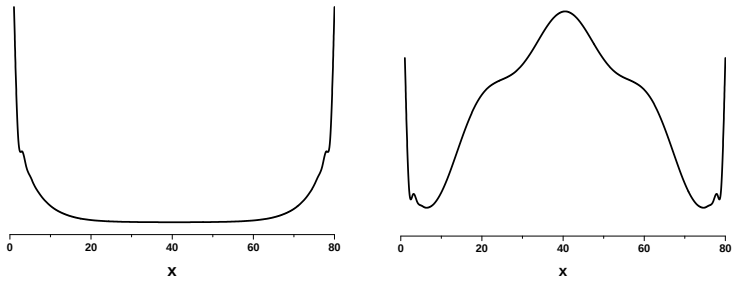

(a) $E_f = 7$ and $W = 0$.

(b) $E_f = 15$ and $W = 0$.

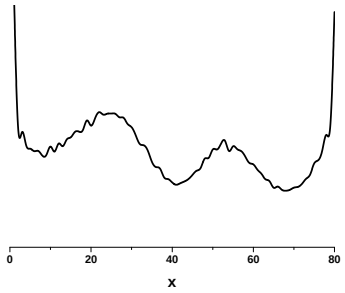

(c) $E_f = 15$ and $W = 50$.

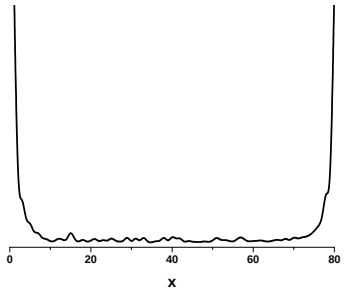

(d) $E_f = 15$ and $W = 100$.

Figure 5.3: Local density of states $\rho(x)$ for a 200×80 lattice in equilibrium, meaning no leads present. For all figures $M = -10$.

5.4 (right) the Fermi energy is in the conduction band and bulk transport exists. But after a transition into the TAI phase (compare with figure 5.1) the bulk states are localized and no local transport is seen, but along the upper edge current is still flowing. The same qualitative behavior is seen when $M > 0$ [21]. Thus we conclude that topologically robust edge states emerges as the result of impurities, which gives rise to a ideally quantized conductance.

5.2 Disorder induced band inversion mechanism

The topological Anderson insulator is a amazing and unexpected state of matter which will hopefully be experimentally observed. So far we have only discussed numerical calculations and an understanding of the underlying mechanism is still missing. The figures 5.1 and 5.2 gives us a few important clues. It is observed that the critical disorder strength W_c is independent of the sample size, but clearly depends on the Fermi energy E_f and the topological mass M. When E_f is in the valence band, TAI is not observed. When E_f is in the conduction band W_c grows for larger E_f, so even bigger disorder strength is required when the Fermi level is farther away from the QSH edge states (the bulk gap). From the figures 5.3 and 5.4 we see that the TAI state looks very similar to the QSH state.

An explanation consistent with these observations is that the chemical potential[6] and the topological mass is decreased because of impurities, so for a fixed W the system has a effective chemical potential $\bar{\mu}$ and topological mass $\bar{M}$. By this way E_f is dragged down to the bulk gap where edge states exists, for larger E_f more "down dragging" has to be done (larger W_c)[7] All

[6] At $T = 0$ the chemical potential is identical to the Fermi energy.

[7] And if the system is in the trivial insulating phase, the topological mass M is decreased to flip sign, so that the system get into the inverted band regime. This creates edge states in the bulk gap.

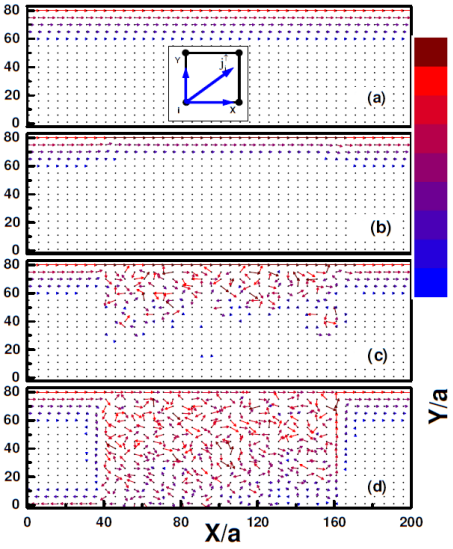

(a) (a) $W = 0$, (b) $W = 50$, (c) $W = 110$, (d) $W = 220$.

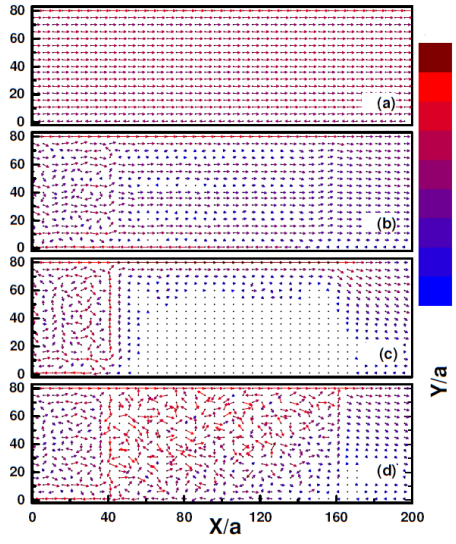

(b) (a) $W = 0$, (b) $W = 65$, (c) $W = 100$, (d) $W = 250$.

Figure 5.4: Local current calculations for a 200×80 lattice with impurities distributed in $40a < X < 160a$. The Fermi energy for the left figure is $E_f = 7$ while for the right $E_f = 18$, furthermore we have $M = -10$ for both figures. Only the spin up subsystem is shown. The colors represent the length of the local current vectors. These figures are taken from [21].

the stated observations can be explained by this idea.

To understand the origin of this mechanism, take the continuum Hamiltonian for the spin up sub-system (3.5) (the spin down sub-system is given by time reversal) and replace $\boldsymbol{k} \to \boldsymbol{p} = -i\boldsymbol{\nabla}$ since the translational symmetry is broken,

$$h = \alpha\left(p_x\sigma_x - p_y\sigma_y\right) + \left(m + \beta p^2\right)\sigma_z + \left(\gamma p^2 + U(x,y)\right)\sigma_0, \tag{5.1}$$

where $\alpha = A$, $\beta = -B$, $\gamma = -D$, $m = M$ have been introduced to keep the signs of the parameters positive (compare with experimental values) and have the same notation as [15]. $U(x,y)$ represents the impurity potentials.[8] Elastic scattering by a disorder potential causes states to become localized, meaning that they will exponentially decay as a function of space $\phi(x,y) \to \phi(x,y)e^{-(x+y)/\lambda}$. Therefore term $\beta p^2\sigma_z = -\beta\nabla^2\sigma_z$ adds a negative correction $-\delta m$ to the topological mass, while the term $\gamma p^2\sigma_0$ shifts the chemical potential. The the renormalized topological mass $\bar{m} = m - \delta m$ may have opposite sign than the bare mass m and effectively cause a phase transition. This idea was proposed by Groth et al. [15] soon after the discovery of the TAI state.[9]

Let H_0 (H) denote the spin-up lattice Hamiltonian for the clean (dirty) system in momentum representation and define a self-energy Σ through

$$\left(E_f - H_0 - \Sigma\right)^{-1} = \left\langle \left(E_f - H\right)^{-1} \right\rangle, \tag{5.2}$$

where $\langle\cdots\rangle$ is the disorder average. Now $H_0 - \Sigma$ can be thought of as an (in general non-hermitian) "effective Hamiltonian". Decompose the self-energy into Pauli matrices $\Sigma = \Sigma_0\sigma_0 +$

[8] Again, these potential are uniformly distributed in the interval $[-\frac{W}{2}, \frac{W}{2}]$.

[9] At this moment, only three papers have been published concerning TAI, namely [28, 21, 15].

$\Sigma_x\sigma_x + \Sigma_y\sigma_y + \Sigma_z\sigma_z$. Groth et al. [15] argue that only the topological mass and the chemical potential are renormalized and given by (compare with equation 5.1)

$$\bar{m} = m + \lim_{k\to 0} \mathrm{Re}\Sigma_z, \qquad \bar{\mu} = E_f - \lim_{k\to 0} \mathrm{Re}\Sigma_0. \tag{5.3}$$

Using the self-consistent Born approximation, Σ is given by the integral equation [15]

$$\Sigma = \tfrac{1}{12} W^2 (a/2\pi)^2 \int \mathrm{d}\boldsymbol{k} \left[E_f + i\eta - H_0(\boldsymbol{k}) - \Sigma\right]^{-1}, \tag{5.4}$$

where the integral is over the first Brillouin zone.

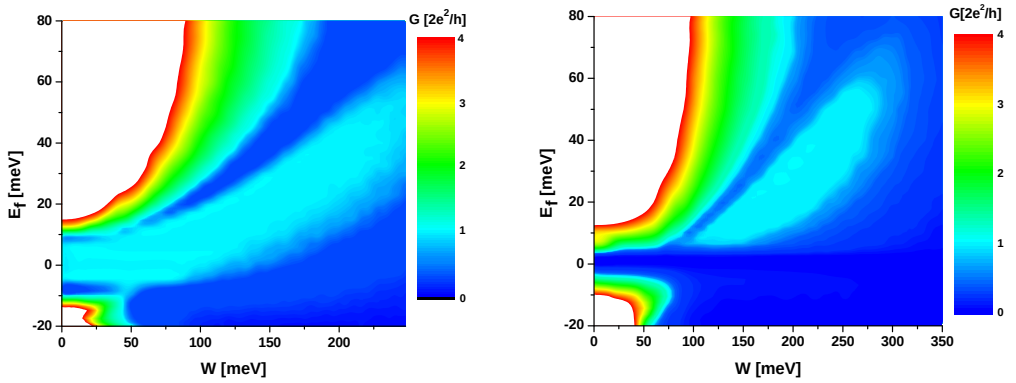

(a) 200×80 lattice with $M=-10$, averages up to 180 times.

(b) 200×90 lattice with $M=1.5$, averages up to 250 times.

Figure 5.5: Phase diagram calculated using the quantum transport code. The blue "islands" correspond to the TAI phase, where $G = 2e^2/h$.

In figure 5.5 the phase diagram is numerically calculated for $M=-10$ and $M=1.5$.[10] Due to time constrain, we have not solved equation (5.4) numerically. But Groth et al. [15] have done so and plotted the two branches corresponding to $\bar{m}$ changing sign and $\bar{\mu}$ being inside the bulk gap (see figure 3.4) as function of E_f and W. Quit amazingly the E_f and W for which these two conditions are fulfilled, corresponds exactly to the areas shown in figure 5.5 (see [15] for more details).

This mechanism for the conversion of an ordinary insulator into a topological insulator is not restricted by dimension, it relies only on the Dirac equation with quadratic momentum terms. Narrow-band semiconductors with strong spin-orbit coupling are generally, for low energies, described by this type of Dirac equations. As discussed earlier, the HgTe/CdTe quantum well has an intrinsic mechanism for band inversion. This is done by changing the well thickness. Other materials described by similar equations may not have any intrinsic mechanism to do this, for these materials disorder can be the key to access topological states. New and exiting topological insulators without an intrinsic band inversion mechanism may be found in the near future.

[10] In figure 5.5 for $M=1.5$ one cannot see any TAI phase when E_f is in the gap. In reality this phase also exists there (for $W\approx100$), but since our lead are exact copies of the sample it is gaped for theses energies. If we had doped our leads or used metallic leads, the TAI phase would be slightly bigger.

Conclusion

In this project we have demonstrated that completely states of matter exist, which cannot be explained by Landau's symmetry breaking paradigm. These states are described by topological invariants which play the role of an "order parameter". We have shown how edge states, the most fundamental property of these phases, are seen in the energy spectrum for both time reversal breaking and time reversal invariant systems.

Furthermore we have build a useful program able to perform non-equilibrium quantum transport calculations. This has been used to study Anderson disorder on the HgTe/CdTe quantum well and the topological Anderson insulating phase was shown explicitly and analyzed. As discussed, this disorder induced band inversion mechanism may proof useful in creating and controlling new topological insulators without any intrinsic band inversion mechanism and thereby expanding the class of topological matter. I am however not sure if it correct to classify the TAI as a distinct phase than the QSH state. The topological "order parameter" are in both cases the same, it is the Z_2 topological invariant and they are clearly not topologically distinct. The TAI is only a new non-intrinsic but disorder induced mechanism to obtain a QSH system. But in the end, it depends on how we choose to define a "phase". Is the topological/symmetrical order the defining element, the mechanism for phase transition or maybe something completely different?

Our program can easily be used to study the TAI and the QSH system even further. For example studying the response to magnetic fields, or magnetic impurities which both are time reversal breaking perturbations.

Quantum transport source code

Bibliography

[1] Altland, A. and B. Simons (2006). *Condensed Matter Field Theory*. Cambridge University Press.

[2] Avron, J. E., R. Seiler, and B. Simon (1983). Homotopy and Quantization in Condensed Matter Physics. *Physical Review Letters 51*(1), 51.

[3] Baez, J. C. and J. P. Muniain (1994). *Gauge Fields, Knots and Gravity*. World Scientific Publishing Company.

[4] Bernevig, B. A., T. L. Hughes, and S.-C. Zhang (2006). Quantum Spin Hall Effect and Topological Phase Transitions in HgTe quantum wells. *Science 314*, 1757.

[5] Berry, M. V. (1984). Quantal phase factors accompanying adiabatic changes. *Proceedings of the Royal Society of London A 392*, 45.

[6] Bohm, A., L. J. Boya, and B. Kendrick (1991). Derivation of the geometrical phase. *Physical Review A 43*(3).

[7] Bruus, H. and K. Flensberg (2004). *Many-Body Quantum Theory in Condensed Matter Physics*. Oxford University Press.

[8] Datta, S. (1995). *Electronic Transport in Mesoscopic Systems*. Cambridge University Press.

[9] Datta, S. (2005). *Quantum Transport: Atom to Transistor*. Cambridge University Press.

[10] Drouvelis, P. S., P. Schmelcher, and P. Bastian (2006). Parallel implementation of the recursive Green's function method. *Journal of Computational Physics 215*, 741–756.

[11] Folland, G. B. (2008). *Quantum Field Theory: A Tourist Guide for Mathematicians*. American Mathematical Society.

[12] Frankel, T. (1997). *The Geometry of Physics*. Cambridge University Press. A second edition exists.

[13] Fu, L. and C. L. Kane (2007). Topological insulator with inversion symmetry. *Physical Review B 76*(045302).

[14] Godfrin, E. M. (1991). A method to compute the inverse of an n-block tridiagonal quasi-hermitian matrix. *Journal of Physics: Condensed Matter 3*, 7843–7848.

[15] Groth, C. W., M. Wimmer, A. R. Akhmerov, J. Tworzydlo, and C. W. Beenakker (2009). Theory of the topological Anderson insulator. *Physical Review Letters 103*(196805).

[16] Haldane, F. D. M. (1988). Model of a Quantum Hall Effect without Landau Levels: Condensed-Matter Realization of the "Parity Anamaly". *Physical Review Letters 61*(18).

[17] Halperin, B. I. (1982). Quantized Hall conductance, current-carrying edge states, and the existence of extended states in a two-dimensional disordered potential. *Physical Review B 25*(4).

[18] Hedegaard, P. Functional Integrals. Lecture notes.

[19] Jauho, A. P. Introduction to the Keldysh nonequilibrium Greens function technique. Lecture notes.

[20] Jauho, A.-P., N. S. Wingreen, and Y. Meir (1994). Time-dependent transport in interacting and noninteracting resonant-tunneling systems. *Physical Review B 50*(8), 5528.

[21] Jiang, H., L. Wang, Q.-F. Sun, and X. C. Xie (2009). Numerical study of the topological Anderson insulator in HgTe/CdTe quantum wells. *Physical Review B 80*(165316).

[22] Kane, C. L. and E. J. Mele (2005a). Quantum Spin Hall Effect in Graphene. *Physical Review Letters 95*(226801).

[23] Kane, C. L. and E. J. Mele (2005b). Z_2 Tological Order and the Quantum Spin Hall Effect. *Physical Review Letters 95*(146802).

[24] König, M., H. Buchmann, L. W. Molenkamp, T. Hughes, C.-X. Liu, X.-L. Qi, and S.-C. Zhang (2008). The Quantum Spin Hall Effect: Theory and Experiment. *Journal of the Physical Society of Japan 77*(3).

[25] Kohmoto, M. (1985). Topological Invariant and the Quantum of the Hall Conductance. *Annals of Physics 160*, 343.

[26] Laughlin, R. B. (1981). Quantized Hall conductivity in two dimensions. *Physical Review B 23*(10).

[27] Lee, D. H. and J. D. Joannopoulos (1981). Simple scheme for surface-band calculations. ii. The Green's function. *Physical Review B 23*(10), 4997.

[28] Li, J., R.-L. Chu, J. K. Jain, and S.-Q. Shen (2009). Topological Anderson Insulator. *Physical Review Letters 102*(136806).

[29] Linder, J., T. Yokoyama, and A. Sudbø (2009). Anomalous Finite Size Effects on Surface States in the Topological Insulator Bi_2Se_3. *Physical Review B 80*(205401).

[30] Marder, M. P. (2000). *Condensed Matter Physics*. Wiley-Interscience.

[31] Meir, Y. and N. S. Wingreen (1992). Landauer Formula for the Current through an Interacting Electron Region. *Physical Review Letters 68*(16), 2512.

[32] Murakami, S. Quantum Spin Hall Phases. *Progress of Theoretical Physics 176*, 279.

[33] Nagaosa, N. (1999). *Quantum Field Theory in Condensed Matter Physics*. Springer.

[34] Nakahara, M. (1990). *Geometry, Topology and Physics* (1 ed.). CRC Press. A second edition exists.

[35] Niu, Q., D. J. Thouless, and Y.-S. Wu (1985). Quantized Hall conductance as a topological invariant. *Physical Review B 31*(6), 3372.

[36] Novoselov, K. S., A. K. Geim, S. V. Morozov, D. Jiang, M. I. Katsnelson, I. V. Grigorieva, and S. V. Dubonos (2005). Two-dimensional gas of massless Dirac fermions in graphene. *Nature Letters 438*, 197.

[37] Qi, X.-L., T. L. Hughes, and S.-C. Zhang (2008). Topological field theory of time-reversal invariant insulators. *Physical Review B 78*(195424).

[38] Roy, R. (2009). Z_2 classification of quantum spin Hall systems: An approach using time-reversal invariance. *Physical Review B 79*(195321).

[39] Thouless, D. J., M. Kohmoto, M. P. Nightingale, and M. den Nijs (1982). Quantized Hall Conductance in a Two-Dimensional Periodic Potential. *Physical Review Letters 49*(6), 405.

[40] van Leeuwen, R. and N. E. Dahlen. An Introduction to Nonequilibrium Green Functions. Lecture notes.

[41] Wakabayashi, K., M. Fujita, H. Ajiki, and M. Sigrist (1999). Electronic and magnetic properties of nanographite ribbons. *Physical Review B 59*(12).

[42] Wen, X.-G. (2004). *Quantum Field Theory of Many-Body Systems*.

[43] Zhang, H., C.-X. Liu, X.-L. Qi, X. Dai, Z. Fang, and S.-C. Zhang (2009). Topological insulators in Bi_2Se_3, Bi_2Te_3 and Sb_2Te_3 with a single Dirac cone on the surface. *Nature Physics 5*, 438.

[44] Zhang, J., Q. W. Shi, and J. Yang (2004). Electronic transport in Z-junction carbon nanotubes. *Journal of Chemical Physics 120*(16), 7733.

[45] Zhou, B., H.-Z. Lu, R.-L. Chu, S.-Q. Shen, and Q. Niu (2008). Finite Size Effects on Helical Edge States in a Quantum Spin-Hall System. *Physical Review Letters 101*(246807).